論文 / 著書情報
Article / Book Information

題目(和文)	
Title(English)	A Basic Study on Weight Estimation of Vehicle in Motion Based on Averaging Method
著者(和文)	PHAMTung Xuan
Author(English)	Tung Pham
出典(和文)	学位:博士（工学）, 学位授与機関:東京工業大学, 報告番号:甲第11911号, 授与年月日:2021年3月26日, 学位の種別:課程博士, 審査員:大熊 政明,坂本 啓,髙原 弘樹,山浦 弘,武田 行生,中野 寛
Citation(English)	Degree:Doctor (Engineering), Conferring organization: Tokyo Institute of Technology, Report number:甲第11911号, Conferred date:2021/3/26, Degree Type:Course doctor, Examiner:,,,,,
学位種別(和文)	博士論文
Type(English)	Doctoral Thesis

A Basic Study on Weight Estimation of Vehicle in Motion Based on Averaging Method

東京工業大学
Tokyo Institute of Technology

Pham Xuan Tung

Department of Mechanical Engineering
Tokyo Institute of Technology

This dissertation is submitted for the degree of
Doctor of Philosophy

Supervisors: Prof. Masaaki Okuma
Assoc. Prof. Hiraku Sakamoto

Tokyo Institute of Technology February 2021

I would like to dedicate this thesis to my lovely wife Thanh Mai and my children Minh Nhat and Minh An . . .

Acknowledgements

I would like to express my special thanks to my supervisor, Professor Masaaki Okuma for his inspiration, support, encouragement and guidance for the full time I was in Japan. I also would like to thank Associate Professor Hiraku Sakamoto for his essential advice for my research. Moreover, I would like to thank all examiners, Professor Takahara, Professor Yamaura, Professor Takeda, Associate Professor Nakano for reviewing my work and giving me very important comments for improving this dissertation. Furthermore, I would like to thank Professor Bur, Professor Abidin, Dr. Meifal Rusli, and Dr. Lovely Son for their valuable discussions. I also want to express my appreciation to Dr. Kawaguchi for his research support, to Mr. Fukai for his collaborative research work.

Regarding financial support, I need to thank JICA for AUN-SEED-Net scholarship. I also would like to thank Ms. Ishii for her assistance for completing a variety of documents, Ms. Britta for English proofreading. Besides, I would like to thank all students from the Okuma-Sakamoto Laboratory for a memorable experience. In addition, I would like to thank my colleagues from Hanoi University of Science and Technology for their encouragement.

Finally, I would like to thank my parents, my wife and my children for their support and encouragement. Thank you for always being beside me at the most challenging time.

Abstract

Measuring the weight of vehicles, especially trucks, moving on a traffic lane with practical accuracy and reliability without making them stop is desirable. More clearly, from the vantage point of road damage protection, traffic safety, and high monitoring efficiency, it is important to establish a system to measure each axle load of a vehicle while it is traveling on the road. This type of vehicle weight measurement is called “Weigh-In-Motion”(WIM) system. The techniques of WIM are classified into “pavement WIM” and “bridge WIM". Pavement WIM is a better choice than bridge WIM due to the wide application. There are load estimation methods, which have been proposed for pavement WIM. However, those algorithms are limited because of time-consuming calibration or high errors of estimation. This research proposes a new estimation algorithm based on an averaging theory using plate-type measurement devices. The algorithm has a unique feature and a unique function. The feature of this research is the estimation with slight underestimate. The function of this method is available for test vehicles not only with constant but also non-constant speeds. The way of using two or more measurement devices placed in cascade layout is found better regarding the reliability and accuracy of the axle load estimation than the usage of a single device. The validity and accuracy of the proposed method are experimentally investigated using motorbikes and a light truck as test vehicles. The results show that the WIM system in this research can estimate the static load of test vehicles with practically acceptable accuracy.

Table of contents

List of figures

List of tables

Nomenclature

Abbreviations

1D	One-dimension
2D	Two-dimension
2DOF	Two degree of freedom
3D	Three-dimension
4DOF	Four degree of freedom
BWIM	Bridge Weigh-in-motion
FE	Finite element
MFI	Moving force identification
WIM	Weigh-in-motion

Symbols

$\bar{V}$	Average speed or average velocity
$_f$	Times when the front wheel gets on the loading plate
$_r$	Times when the rear wheel gets on the loading plate
$\propto$	Damping factor of the bounce and/or pitching mode
$_f$	Times when the front wheel gets off the loading plate
$_r$	Times when the rear wheel gets off the loading plate
ρ	Density of air

τ_1	Times when signals cross the threshold level in the upward directions
τ_2	Times when signals cross the threshold level in the downward directions
$\widehat{t_k}$	Time of local maxima, with k = 1, 2...
A	Accelerated rate
C_D	Aerodynamic drag coefficient
C_L	Aerodynamic lift coefficient
F_D	Aerodynamic drag force
F_L	Aerodynamic lift force
f_n	Natural frequency of the bounce and/or pitching mode
f_s	Sampling rate
g	Gravitational acceleration
h	The height of center of pressure above the level of center of gravity
h_G	The height of the center of gravity above the ground
L	Wheel base
N_f	Normal reaction forces from the ground to the front wheel
N_r	Normal reaction forces from the ground to the rear wheel
N_{tr}	Transfer load
S	Driving force
W_s	Static weight
$\breve{t}_n$	Time of local minima, with n = 1, 2...

Chapter 1

Introduction

1.1 Background and motivation

At present, because of fast economic development, there is a high demand for cargo transport, especially road transport due to its low deleverage time, cost and its flexibility. However, due to profits, freight companies tend to not comply with the load regulations, leading to an increase of overloaded vehicles on the road. It has caused negative economic and social impacts, which are mainly the destruction of road structures and bridges, potential risks of traffic accidents, and the creation of an environment with unequal competition between the transport companies. Firstly, overload trucks mean the trucks carry large quantities of goods, which exceed the permitted volume. Because of that overweight, they often damage roadways (Fig. 1.1). According to the reports of Departments of transportation of New York, Arizona and Indiana [1–3] the costs of damage to their pavements from overweight trucks are approximately $145 million, $210 million, and $354-397 million per year, respectively. Since road maintenance is costly, that problem has serious impacts to the economy. Secondly, overloaded trucks are at high risk of causing serious traffic accidents. Because their center of gravity is higher, leading to a high risk of them to rollover as depicted in Fig. 1.2. Furthermore, if the position of the gravitational center is closer to the front axle than the rear axle or vice versa, it can lead to locked wheel status [4]. Thirdly, over-weight trucks can also cause unfair competition between carriers. Freight companies, who use more overloaded trucks can push other fair companies out of the market, leading to bankruptcy.

Therefore, it is important to reduce the number of overloaded vehicles on the road by facilitating vehicle weight inspection. Traditionally, the static weighing station is used to measure the static weight of trucks (Fig. 1.4) [5]. However, static weighing has some limitations. First, the establishment of static weighing stations requires staff to operate the measurement system manually. It can be costly and a waste of human resources. In addition,

Fig. 1.1 A damaged road because of overload trucks

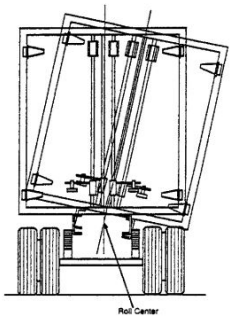

Fig. 1.2 Truck rollover factor[4]

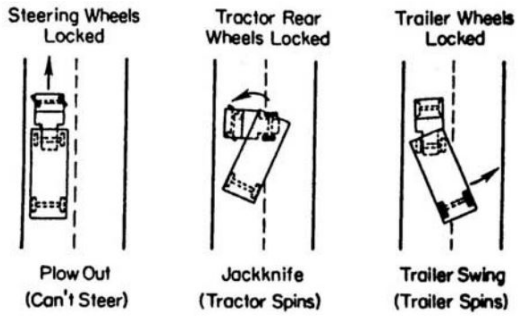

Fig. 1.3 The locked wheel crashes[4]

static weighing is time-consuming and stopping the traffic flow on the road can lead to the traffic congestion. That is particularly impractical on heavily trafficked roads like highways.

As a results, it is desirable to establish a system to measure each axle load of a vehicle while the vehicle is moving on the road. This type of vehicle weight measurement is called "Weigh-In-Motion" (WIM). It is aimed at measuring the static weight of all trucks moving in the flow of traffic without stopping them. Therefore, compared with static weighing, WIM technology has several advantages. The biggest one will be the possibility of inspecting all passing trucks.

The WIM system is a system that incorporates some components related to the weight of the axle/wheel of vehicle. It is classified into two main types: bridge WIM (BWIM) and pavement WIM (or simply WIM) [5]. BWIM utilizes bridges as a scale to measure the dynamic force of vehicle by processing the signals of sensors, which are installed on the

Fig. 1.4 Static measurement

bottom side of the bridge, or culvert. The passing vehicle causes bending of the bridge, and the occurring strain can be measured by the sensors such as accelerometers or strain gauges (Fig. 1.5) [6].

Pavement WIM or WIM typically uses the force sensors which are installed at the same level with the road's surface (Fig. 1.6). They are oriented perpendicularly to the travel movement to measure the dynamic load of vehicles [4] (Fig. 1.6). Pavement WIM can be classified according to the range of velocity criteria or the size of the measurement devices. Based on the speed, WIM divides into high-speed WIM with the velocity of vehicle V is faster than 15 km/h and low-speed with velocity is slower than 15 km/h [7]. According to the size of the measuring device, WIM divides into two main types: scales/plates and strip/bar sensors. WIM scales/plates have a length of 0.3 to 0.8 m in the traveling direction, and a width of either is shorter than 1 m (wheel weight) or longer 3 m (axle weight). On the other hand, piezoelectric strip/bar sensors such as ceramic, polymer or quartz sensors are the most popular for pavement WIM. Strip sensors have a length of 2 to 7 cm in the traffic direction and a width of approximately 1 to 6 m of the traffic lane (Fig. 1.7). The advantages of strip sensors are low-cost, easy to install, and maintain [5].

Compared to pavement WIM, BWIM has both advantages and disadvantages. On the one hand, because BWIM sensors are installed under the bridge, they do not have direct contact with the impact forces from the vehicle, resulting in longer durability than the pavement WIM sensors. Moreover, the installation of BWIM sensors is easier, safer, and does not need temporal closure of the road, therefore it does not affect the traffic flow. On the other hand, they also have some disadvantages. Firstly, the application of BWIM is limited because they

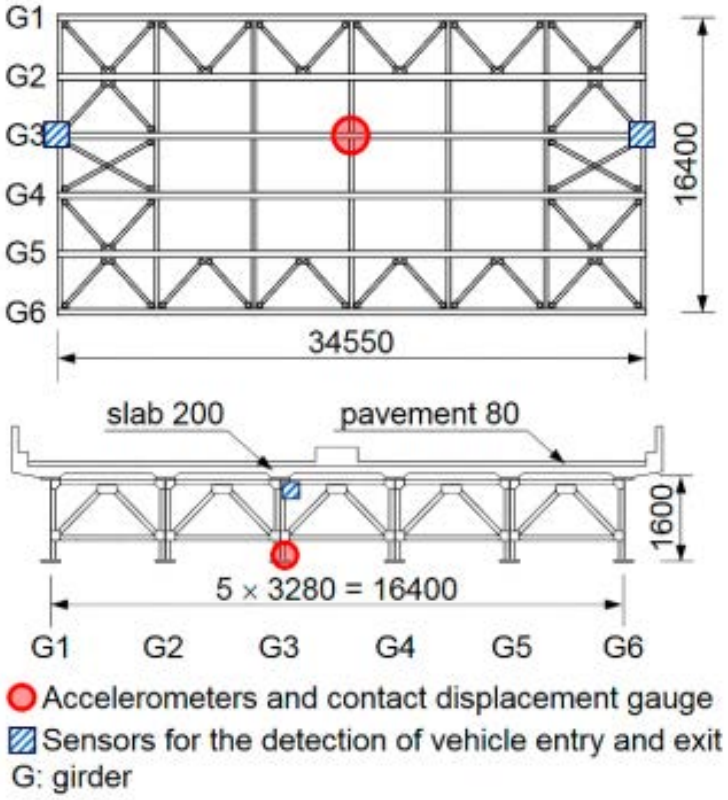

Fig. 1.5 Bridge Weigh-In-Motion [6]

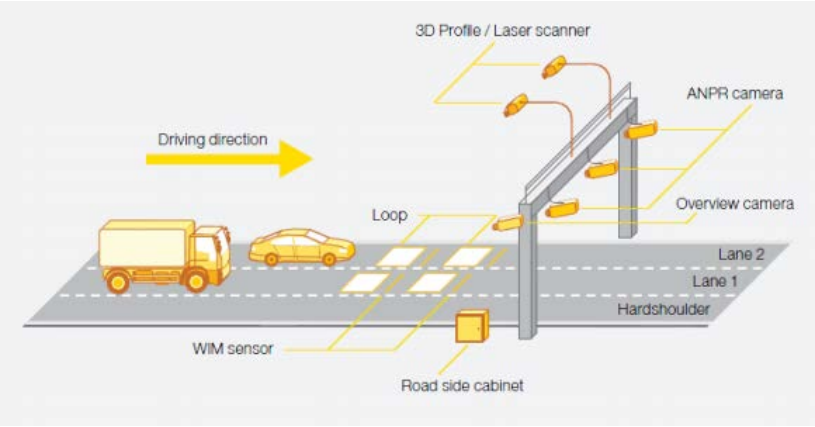

Fig. 1.6 A type of Weigh-in-motion system [8]

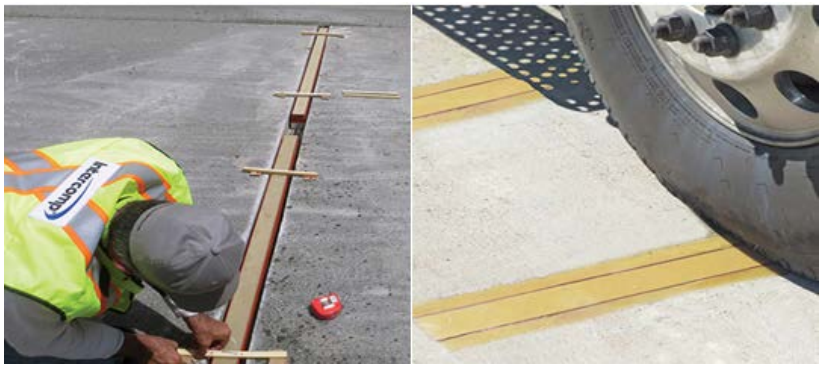

Fig. 1.7 Strip sensors (Copyright by Intercomp)

use bridges as a measurement device. It is applicable only in places that have a bridge or a culvert. Secondly, when there are two or more vehicles moving on the bridge, the signal from the sensors will get interference, which makes it difficult to separate not only axle weights but also gross weight of each vehicle. Although there are several drawbacks, BWIM is still being developed and researched with the aim of monitoring the bridge health structure, for the purpose of predicting failures, maintaining bridges. It is also used for collecting traffic flow on bridges for development and anticipating the demand of transport infrastructure.

Basically, pavement WIM uses sensors to measure the value of dynamic loads of vehicles, and then estimate the static weights. In addition to the main component is, a force sensor, pavement WIM also uses other sensors to assist the static weight estimation and to collect information about the vehicle. Those are loop sensors which are used to define the distance between axles, velocity and wheelbase. The average velocity and the distance of axle are calculated by using the traveling time and the distance between loop sensors as below

$$\bar{V} = \frac{Distance\ of\ loop\ sensor}{Travelling\ time} \tag{1.1}$$

$$L_{axle} = \bar{V} \times\ period\ of\ time\ between\ two\ axles \tag{1.2}$$

Through parameters such as axle distances, axle weight, combined with image or video processing identification, the vehicle classification system will recognize the type of vehicle and provide standard static load requirements (Fig. 1.8)

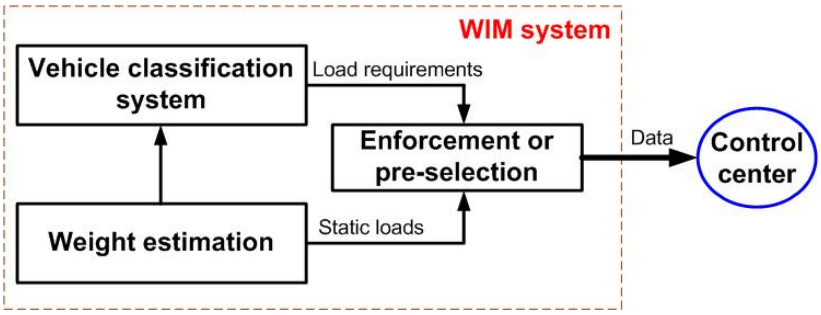

Fig. 1.8 Principle of a WIM system

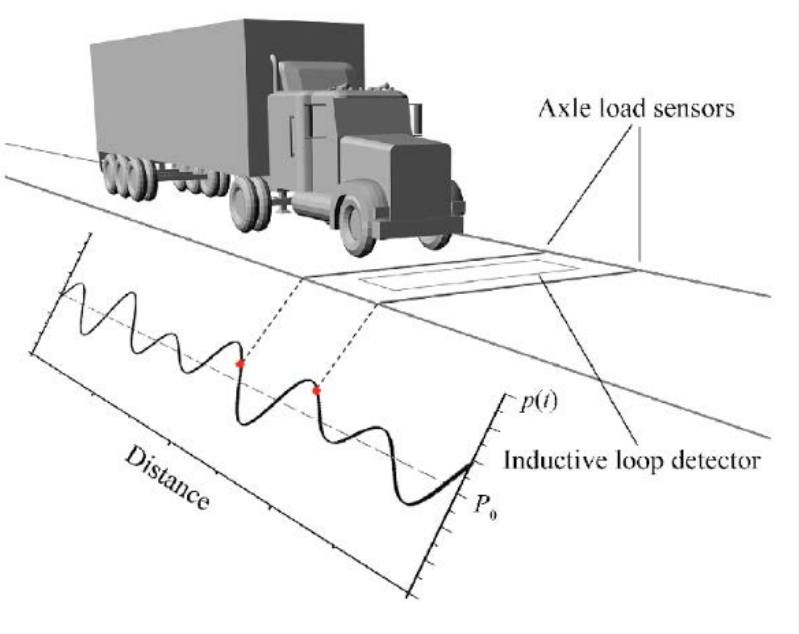

Fig. 1.9 Short time history signal [9]

1.2 State of the arts of WIM

The essential development point of WIM is how to realize an accurate and reliable estimation of static weighing of vehicles from the sensor signals composed of both static and dynamic loads, such as shocks and vibrations at various vehicle speeds. A dynamic load is generated in many ways, such as impulses at the moment when a wheel moves onto and off the measurement device, a vehicle's vibration due to suspension characteristics and movement, and the inherent dynamics of the measurement device. Furthermore, the very short duration of time that the axle load is on the measurement device makes it extremely difficult to estimate the static weight, especially in the case of a high-speed vehicle (Fig. 1.9). For example, it the length of a measurement device in traveling direction is 1 m, and the speed of a vehicle is around 50 km/h, the time history signal is approximately 0.07s.

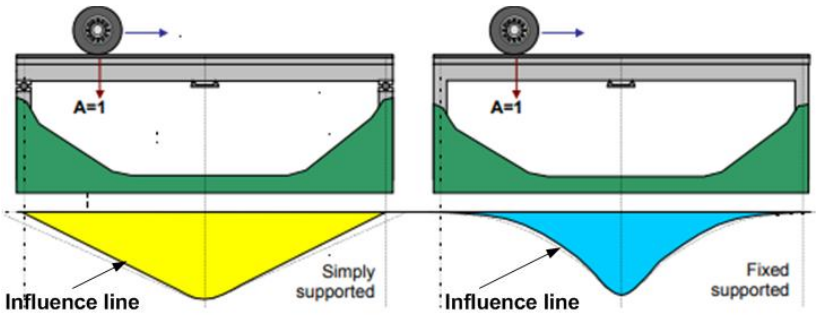

Fig. 1.10 Influence lines for simply and fixed supported bridge [13]

Currently, there are two mainly standard accuracy specifications for WIM systems, namely COST 323 [10] and ASTM E1318-09 [11]. The COST 323 is the most popular practical use. It is established by European Cooperation in Science and Technology project. COST 323 classifies the assessment of WIM accuracy into seven classes in which B(10) and C(15) classes mean the estimation errors of less than 10% and 15% in 95% measured data respectively, and recommends from B(10) to A(5) classes as being suitable for enforcement or pre-selection.

Table 1.1 Accuracy specification (COST 323)

Class	A	B+	B	C	D+	D	E
Errors	5	7	10	15	20	25	30

BWIM technique

There are two main estimation methods for BWIM: one method is based on influence lines combining regularization technique, and the other is based on moving force identification (MFI). The theory of static load estimation for BWIM was first proposed by Moses [5]. This algorithm is based on the bridge responses (strain or displacement) when a vehicle passes over the bridge. In theory, the influence line $l(x)$ is determined by measuring the response of the structure when being acted by a load at x position. Moses' estimation algorithm assumed that if the structure behaves are linearly and ignoring dynamic responses, the bending moment M_{th} is proportional to the load W and the influence line of the bridge I (Fig. 1.10) [12].

The bending moment from the sensors at time step k:

$$M_k^m = \sum_i^{N_g} ES_i\varepsilon_i \tag{1.3}$$

where N_g is the number of girders, E is the elasticity, S is the section of girder, ε is the measured strain.

The theoretical bending moment (based on the influence line):

$$M_k^T = \sum_i^n A_i I_{(k-C_i)} \tag{1.4}$$

$$C_i = \frac{B_i f_s}{V} \tag{1.5}$$

where n is the number of axles, A is the weight of the axle, $I_{(k-C_i)}$ is the influence ordinate at the position of the ith axle, B_i is the distance between the axle ith and first axle, C is the number of scans, f_s is the sampling frequency, and V is the vehicle speed.

The error between theory and measurement [14] is :

$$E = \sum_{k=1}^{N} \left(M_k^T - M_k^m\right)^2 \tag{1.6}$$

The load estimation is obtained by solving the error function by using least-square.

However, the disadvantage of this algorithm is the inaccurate caused by the difference in behavior between the theoretical model and real bridges. There are some major factors that affect the accuracy of prediction such as complex dynamic behavior of a vehicle, the transverse position of a vehicle and ill-conditioned equation due to the rough road surface [12]. To overcome this issue, some algorithms are studied to improve the estimation result. Instead of a 1D influence line, a 2D influence surface is proposed to improve the estimation algorithm [15]. The disadvantage of this method is the time-consuming calibration and computer load for the accuracy of the finite element (FE) model of bridges. Moreover, some studies [16, 17] demonstrate that the Tikhonov regularization with Moses' algorithm can be utilized to deal with ill-conditioned equation. Although the papers reported the good results, the convergence of solution is slow. Moreover, the influence line plays an essential role in BWIM estimation algorithm, methods to extract it from measurement data have also been studied. Karoumi et al. [18] presents an influence line extraction method by using an inverted matrix based on a calibration vehicle. Frøseth et al. [19] proposed the extraction of influence line based on the FFT algorithm and a regularization technique.

The MFI is the second main method to estimate the static weight of a vehicle for BWIM. This method pursues to find the time history of dynamic force when a vehicle travels over the

bridge [12]. Based on Euler's theory or beam element model, solutions can be investigated by applying the least-square method [20], in time-domain [21], in frequency-time domain [22], or based on the finite element and wavelet decomposition [23–25]. Liu et al. [26] also proposed the explicit form based on Newmark-β algorithm to solve the problem of force identification. The results are more accurate compared with the conventional explicit method, especially with a low sampling frequency. Moreover, instead of 1D and 2D models, the solution for 3D finite element of a bridge is also studied [27, 28]. However, the drawbacks of the MFI methods are still based on simple bridge models and time-consuming computation.

To summarize, the estimation methods for BWIM has some limitations. While the method of using the influence line in combination with the regularization technique still has a high error, the implementation of MFI method for a complex bridge structure is time-consuming, which is not feasible with real-time monitoring.

Pavement WIM technique

The strip/bar sensors are most popular for pavement WIM systems. However, since the size is much smaller than that of a tire's imprint, the sensor signal cannot express the total distributed load in a tire's imprint area. Figure 1.11 shows the relationship between WIM signal and imprint size when a vehicle passes a strip sensor. As can be seen in the graph, tire pressure and tire's imprint play an important role in influencing the output signal. When the dynamic vibration is ignored, the area under the curve can be considered to correspond to the relationship between imprint and force. Figure 1.12 shows the relationship between the WIM signal and the velocity of the vehicle. When the speed increases the peak of WIM signal does not change, but the widths of the signal become narrower [29]. Note that the figures only show the cases of a non-dynamic effect. Therefore, the static load estimation from such a sensor signal significantly depends on vehicle speed, tire pressure, road profiles, vehicle suspension systems and some other factors [30, 5, 31].

The load acting on the sensor can be calculated by [32]

$$W = (V/d) \times A \times C \tag{1.7}$$

where W is wheel load, V is speed of vehicle , d is sensor width, A is area of output signal under the curve and C is calibration parameter.

In order to estimate the static weight of vehicles, the calibration process is very important for this type of WIM. Because the static load estimation depends on many factors, the calibration needs a very long time, and many tests using various vehicles for references.

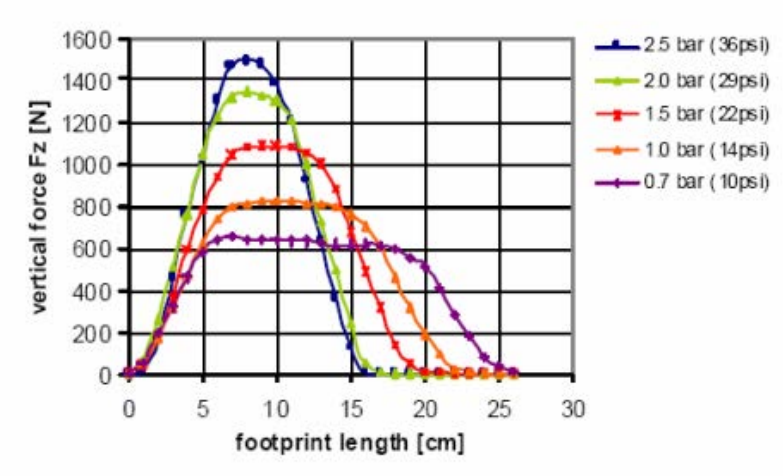

Fig. 1.11 Footprint lengths per varying tire inflation pressure [29]

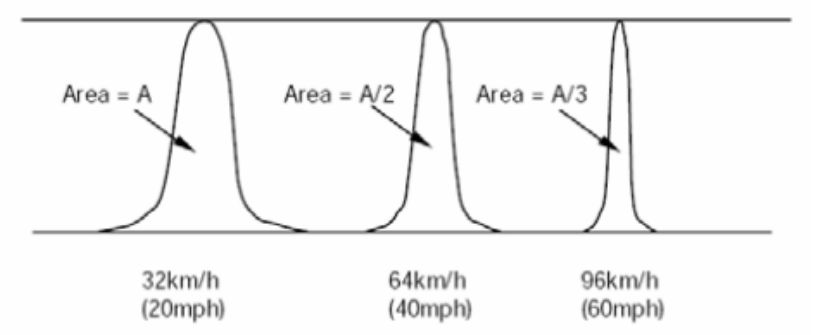

Fig. 1.12 WIM signals on different speeds [29]

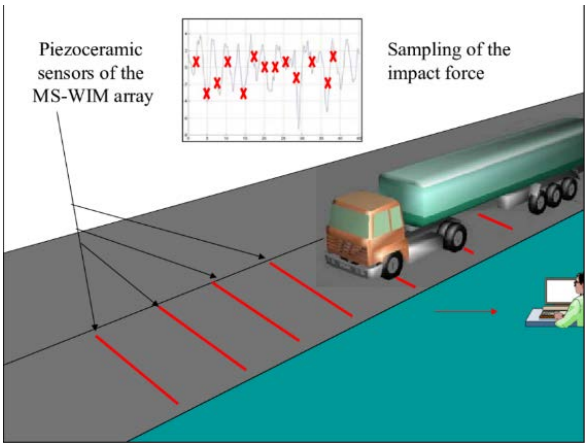

Fig. 1.13 Output signals of MS-WIM sensors [36]

Some researchers reported that it took a very long time from 6 to 12 months using a variety of trucks for the calibration procedure [33, 34]. However, the achieved accuracy of estimation was still not good enough, with mean errors of about 20%, standard deviation errors are approximately 8-19% [34]. Interestingly, the paper [33] mentioned that in cases of trucks running with acceleration and deceleration conditions, the commercial WIM system did not work. Kwon [29] studied on the static load estimation for Kistler sensors by applying 3 methods of signal processing: using the peak output signal, the area under the output signal and re-sampling of the area. However, the results had large errors because of signal noises and vehicle dynamic. Importantly, because the size of the sensor is much smaller than the tire's imprint, it seems to be impossible to estimate or measure the static axle load of the truck in a stationary condition. Multiple sensors Weigh-in-motion (MS-WIM) are developed to increase the accuracy of static load estimation for strip sensors. Figure 1.13 shows a MS-WIM system. The output data signals from MS-WIM sensors are discrete points (red cross marks). The theory of multiple sensors for WIM was first proposed by Cebon et al. [35] in 1990s. Because vehicles have a low natural frequency, the strip sensor cannot record the one period vibration of vehicles. The authors assumed that the vertical dynamic part of a vehicle running with constant speeds was a sinusoidal force. Based on their theoretical assumption, the sensor spacing was proposed. An experiment with 96 sensors was conducted with root mean square error of 4%.

Stergioulas et al. [37] proposed a method for multiple WIM based on the maximum likelihood (ML) method. In that study, the authors proposed a new model dynamic force for vehicles, which was a sum of two sinusoidal functions. Those oscillations were caused by a low-frequency body pitch, a bounce vibration (1.5-4.5 Hz) and an axle-hop vibration (8-15 Hz). Although that research has a good result by simulation, it had practical problems

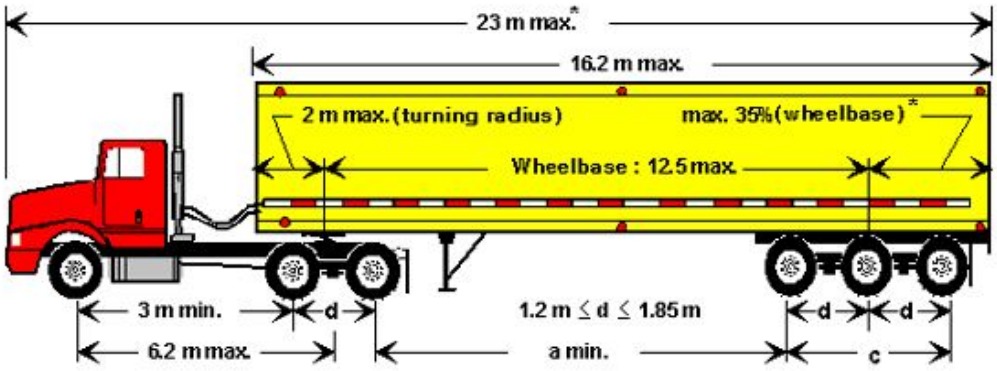

Fig. 1.14 Axle spacing limit [40]

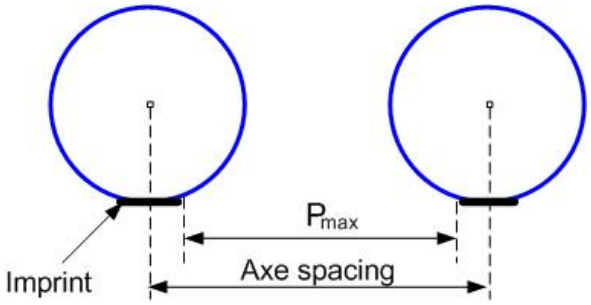

Fig. 1.15 Maximum length of scale/bending plates

because of errors of WIM sensors, such as signal noise, tire effects and calibration. That theory design was implemented, and the accuracy assessment was investigated on the real road in Poland [38] with 16 force sensors. The error of estimation results of gross weight was not exceeding 4% but the system needs a strict periodic calibration.

Compared to strip sensors, scales/bending plates are less popular because of the time-consuming for road construction. Thus, there is not much research on load estimation algorithm based on this type of WIM. Typically, the maximum length of scales/plates in the traveling direction of the vehicle is minimum axle spacing subtracted with the size of wheel/tire imprint to avoid measuring load from two axes at the same time. According to the limit size standard of a vehicle [39], the minimum axle spacing is normally 1.2 m (Fig. 1.14). The wheel/tire imprint is approximately 0.3 m ([5]). Therefore, the maximum length of plates P_{max} is about 0.9 m (Fig. 1.15).

Imakura et al. [41] studied the estimation method based on signal processing using a miniature measurement device with the size of 76 cm. The authors investigated the estimation algorithm with the assumption that the dynamic component of an axle is a sine wave. The parameters of the dynamic component are obtained by applied finite impulse response (FIR).

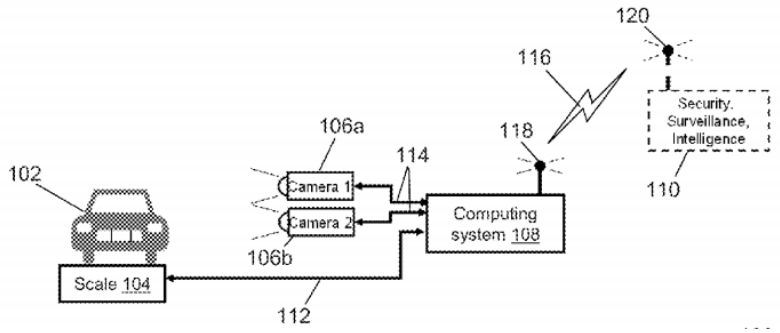

Fig. 1.16 WIM system based on a scale and image processing [43]

However, the study is still limited because the estimation method has not been applied to a real vehicle. There is also a study with a platform, which is larger than the minimum axle spacing. Fukuda et al. [42] studied estimation algorithm with the size of a weighing platform up to 2.2 m. However, because the size of the measurement device is longer than axle spacing, the output signals from the experiments with a 3-axles truck interfered. The authors used a specific notch filter to deal with that problem. Although the estimation results are less than 8%, the limitation of this study is the time-consuming construction process, complicated signal separation algorithm.

Instead of using common force sensors, there are some studies on static load estimation based on new sensor technology. An estimation method combining a scale and stereo vision system was proposed [43] (Fig. 1.16). Using image processing from 2 cameras can obtain the vertical dynamic vibration. The static load is estimated by subtracting the weight from the scale and the vertical dynamic load. However, to the author's knowledge, this solution has not been implemented in practice so far. In addition, because of the image processing, the system will depend on the light source, image quality and the traffic flow. These factors will highly influence the estimation results. Liu et al. [44] investigated the sensor technology based on microwave resonance with considerations of cost and easy installation of equipment on the road. The pressure acting on the wall of the cavity will change the resonant frequency. By determining this changing frequency, the applied force will be calculated. However, this research was only in the laboratory environment. Another research WIM technology based on acoustic emission was studied [45]. The benefit of this technology is its portability and low cost. However, the errors of estimation were high, with a maximum error of 44%. Bajwa proposed an estimation method based on a "pavement-vehicle interaction model", relating the axle load to the vibrations of a pavement, vehicle speed and temperature [46]. The disadvantage of the method is the requirement of a large number of test runs to build a model for each specified measurement site.

Overall, WIM systems are necessary to reduce the number of overload trucks. Due to the wide application, axle weight estimation algorithm, pavement WIM is a better choice than BWIM. However, the current pavement WIM technology still has problems relating to sensor technology and the accuracy of estimation methods. Although the strip sensors are popular, it seems to be not good to develop an estimation algorithm based on that kind of sensor because of the time-consuming calibration. Other sensor technologies such as microwave resonance or acoustic emission is not practical use due to their high errors. To avoid the problems of time-consuming calibration and estimation algorithm, the measurement device needs to be developed with enough size to cover the tire imprint and non time-saving calibration. Pavement WIM with scale/plates type is suitable for those requirements.

More importantly, as far as I know, there is no research, which has specifically investigated estimation algorithms based on an averaging method. In addition, there is also no research investigating the load estimation of a vehicle in motion in cases of acceleration and deceleration. The current commercial WIM systems are invalid for those cases [33]. Thus, it is essential to do research on static load estimation algorithm based on an averaging method for vehicle in motion in cases of constant and non-constant speeds.

1.3 Objectives

Based on the state-of-the-art in the last section, it can be seen that current studies on pavement WIM face many limitations on estimation algorithms. Although the strip/bar type sensors are widely used due to the advantages of road construction, the use of this type of sensor is still limited because its size is much smaller than the tire imprint of vehicles. The weight estimation depends on many factors such as velocity, type pressure, and the road surface. As a result, the calibration process is time-consuming and costly but still does not guarantee accuracy. Besides, research-based on sensors such as accelerometers or acoustics emission has problems such as time-consuming calibration and high errors because they depend significantly on the environment.

In contrast, a plate-type sensor has a size, which is bigger than the imprint size of a vehicle, and smaller than the minimum distance between the two wheels. Therefore, it ensures the entire load is recorded and avoids signal interference. Moreover, because the size of the plate-type is larger than the size of the tire imprint, the calibration process takes a short time and cost-effective. If a plate-type measurement device is designed for the sensor output to be insensitive to the position of the load on the loading plates, the static axle load can be expressed as a rectangular function. As a result, the output signal vibrates around the static load. It is a high potential to apply the averaging theory to estimate the static axle load.

Current studies assume a vehicle moves at a constant speed when it passe through the measurement device. Unfortunately, it does not always move at a constant speed. Therefore, research with non-constant speeds needs to be conducted. The problems with the non-constant speeds are short-time history signals, high dynamic, and a variety of vehicle's parameters. However, we can solve this problem based on the basic dynamic of a vehicle, the signals obtained from the WIM system and some assumptions.

The standard specifications COST 323 is the most popular for the WIM system. As mentioned in the last section, recommends from B (10) to A (5) classes as being suitable for enforcement or pre-selection in practice. Although this study is only a basic study of the WIM system, it is necessary to follow the evaluation of estimation based on that requirement. B(10) class is chosen as a reference to evaluate the estimation results.

Considering the essential point at the preliminary stage is to focus on the critical factors to be clarified, a miniature WIM system was constructed for a motorbike to conduct an experimental investigation. The benefit of using a miniature system is low-cost, time-saving, and compact as well as an easy arrangement of the experimental course. The results will be applicable for the development of another device for a light truck at the next stage, and a full-scale system in the future.

In addition, the difference between a motorbike and a light truck are factors such as driver behavior, steering characteristics, and bike-body behavior in accelerating and decelerating modes. Those factors will change the front and rear load more significantly on a motorbike than on trucks or cars. By conducting experiments with motorbikes and light trucks, it helps to fully evaluate the static estimation algorithm before applying the system to the real road.

Therefore, the research objectives are:

1. Development of load estimation algorithm using a plate-type of sensor:
    - A new estimation algorithm based on an averaging theory
    - Available for constant and non-constant speeds
    - Estimation errors smaller than 10% for 95% of measured data (for a truck).
2. Investigation of feasibility and effectiveness of the load estimation algorithm experimentally using motorbikes and a light truck.

1.4 Organization

The rest of this thesis is organized as follows.

Chapter 2 clarifies the algorithm based on averaging theory to estimate static axle load. An estimation algorithm with unique characteristics and unique functions is proposed in this research. The characteristics are the estimation with slight underestimate. The function is the availability of estimating not only test vehicles at constant speeds but also at accelerative motion and deceleration. When using two or more measurement devices placed in cascade layout is found to increase the reliability and accuracy of the axle load estimation compared to the usage of a single device.

Chapter 3 presents the development of miniature measurement devices for conducting experiments using motorbikes and a light truck. The first version of the device is a plate-type device with a lever mechanism configuration, while the second one is a plate-type device using four load cells. The second version shows the advantages with respect to signal-noise-ratio, linearity, and damping ratio. The measurement device for a light truck is developed according to the knowledge obtained through the experimental studies using the first and second measurement device.

Chapter 4 investigates feasibility and effectiveness of the load estimation algorithm by experimentally using motorbikes and a light truck. Experiments using motorbikes are conducted in walking-mode and driving-mode. The experiments in walking-mode are conducted for the most basic investigation because the motorbike crosses the measurement plate very slowly and avoids the influence of engine vibration, etc. In driving-mode, experiments with constant speeds, acceleration and deceleration are carried out using single and two devices in cascade layout. Experiments using a light truck are conducted to measure the right side wheel load and left side wheel load separately due to the limitation of the experiment. As a result, it is found that the WIM system in this research can estimate the axle loads of test vehicles with acceptable accuracy in accordance with B(10) in the guideline of COST-323 (one of the word standards).

Chapter 5 presents the conclusions of this research with some comments about future works.

Chapter 2

Estimation method

The vertical force of vehicle passing on the loading plate includes the static and dynamic parts. The dynamic part is a complicated part depending on many factors such as suspension systems, road profile, vehicle's speed. Besides, the measurement device has its characteristics, which influence the output signal of sensors. Static load estimation is an algorithm to estimate the static load of a vehicle from the measured data by subtracting the dynamic part, noise components. Therefore, understanding the basic dynamic of a vehicle is essential. There are two ways to simulate the dynamic behavior of cars or motorbikes, which are: half-car and quarter-car in cases of longitudinal movement without the effects of roll motion. The quarter-car model is the simplest model based on the spring-mass-damper system. This two degree of freedom (2DOF) investigates the dynamic performances of vehicle suspension related to road profile (Fig. 2.1a). The half-car model is four degrees of freedom (4DOF) based on spring-mass-damper, and a chassis connecting two wheels to investigate the influences of pitch motion (Fig. 2.1b)[47].

However, if the road or test course has a good profile, and the road/approach and the measurement device has the same surface, the influence of the suspension system is small. Therefore, at the initial stage, the vertical vibration is ignored to simplify the problems of the load estimation algorithm. The influence of constant speed and accelerated conditions is investigated. Based on the characteristics of vertical force acting on a loading plate and output signals of the measurement device, the estimation algorithm is proposed by applying averaging method. The improvement of axle weight estimation algorithm is also studied later to enhance the results of estimation.

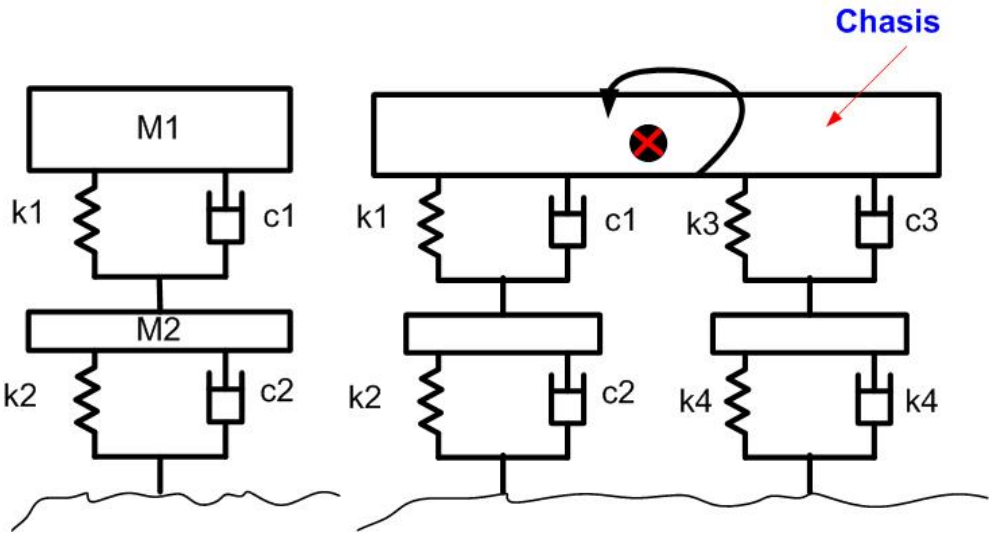

(a) A quarter-car model (b) A half-car model

Fig. 2.1 Simulation of the dynamic behavior of a ground vehicle

2.1 Basic dynamic force balance of ground vehicle for WIM

Ignore the vertical vibration of the vehicle, the basic dynamic force balance of a motorbike is clarified here with a half-car model. Note that the model of truck (one side) is similar. The dynamic force balance during movement is composed of factors such as the driving force by engine power in "driving mode" or the human pushing force in "walking mode" (for motorbike). Other factors include the gravitational force, normal reaction force from the ground to tire, inertia force of the vehicle and a driver under accelerating or decelerating conditions, and aerodynamic forces as shown in Fig. 2.2a for "walking mode" and Fig. 2.2b for "driving mode". These force factors affect the results of static axle load estimation.

Under stationary conditions, the force balance equations of the motorbike are expressed by:

$$mg - N_r - N_f = 0 \tag{2.1}$$

$$N_f (L - b) - N_r b = 0 \tag{2.2}$$

where N_f and N_r are the normal reaction forces from the ground to the front and rear wheels, respectively; L is the wheelbase of the vehicle; b is the horizontal distance between the rear

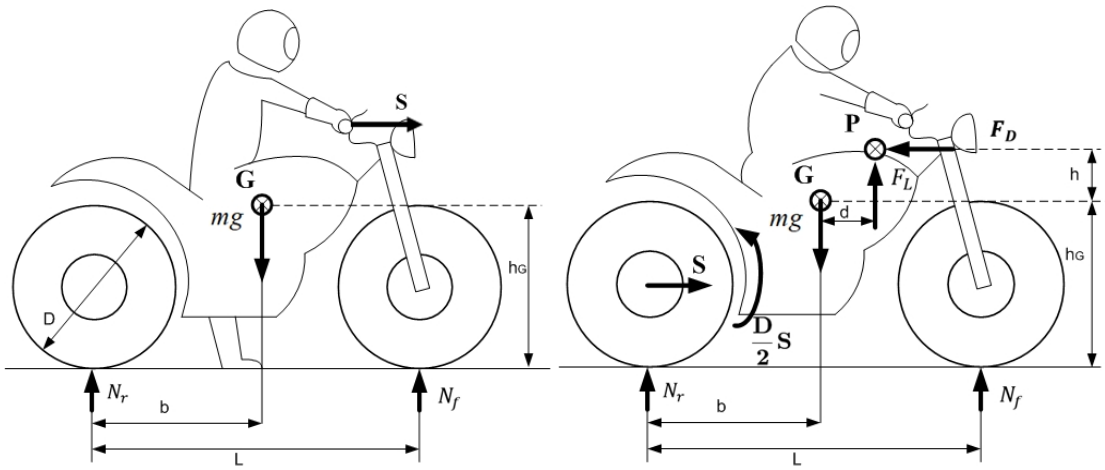

(a) Walking mode (b) Driving mode

Fig. 2.2 Force acting on vehicle in rectilinear motion

Note: G is center of gravity, P is center of pressure, S is driving force, N_r and N_f are the normal reaction forces from the ground to the wheels, respectively, g is the gravitational acceleration, L is the wheel base, and b is the horizontal distance between the rear tire center and the G point, h_G is the height of the center of gravity above the ground, h is the height of center of pressure above the level of center of gravity)

wheel contact point of N_r and G; G is the center of gravity; g is the gravitational acceleration; and the static weight of the front and rear wheels are N_f and N_r, which can be obtained from Eqs.2.3 and 2.4).

$$N_f = \frac{b}{L}mg \tag{2.3}$$

$$N_r = \frac{(L-b)}{L}mg \tag{2.4}$$

Under the accelerated moving condition shown in Fig. 2.2b, the dynamic force balance equations are expressed by Eqs. 2.5, 2.6, and 2.7

$$S - F_D - m\ddot{x} = 0 \tag{2.5}$$

$$mg - N_r - N_f - F_L = 0 \tag{2.6}$$

$$Sh_G - N_r b + N_f (L-b) + F_D h + F_L d = 0 \tag{2.7}$$

Here, we assume that the vehicle moves on horizontal ground, and there is no vibration in the vertical direction. The gross mass of the vehicle and the rider is denoted by "m", while S is driving force, and F_D and F_L are the aerodynamic drag force and lift force acting on the vehicle. F_D and F_L are expressed as

$$F_D = \frac{1}{2}\rho C_D A V^2 \tag{2.8}$$

$$F_L = \frac{1}{2}\rho C_L A V^2 \tag{2.9}$$

where ρ is the density of air; parameter A is the frontal area of the vehicle, C_D and C_L are the aerodynamic drag coefficient and lift coefficient, respectively, and V is the velocity of the vehicle. Thus, the normal reaction forces of the ground to two wheels are

$$N_f = \frac{b}{L}mg - \frac{h_G}{L}S - \frac{h}{L}F_D - \frac{b+d}{L}F_L \approx \frac{b}{L}mg - \frac{h_G}{L}S \tag{2.10}$$

$$N_r = \frac{(L-b)}{L}mg + \frac{h_G}{L}S + \frac{h}{L}F_D - \frac{L-(b+d)}{L}F_L \approx \frac{(L-b)}{L}mg + \frac{h_G}{L}S \tag{2.11}$$

Driving force S is also determined below

$$S \approx m\ddot{x} \tag{2.12}$$

Equations 2.10 and 2.11 show that the normal forces N_f and N_r in driving motion are different from those from the stationary condition. Load transfer occurs between the front and rear wheel. Note here that F_L and F_D are small and negligible for the legal speed range of vehicles on public roads. The value of the load transfer from the front wheel to rear wheel is called the “transfer load”, which is denoted by N_{tr} here, and is expressed as

$$N_{tr} = \frac{h_G}{L} m\ddot{x} \tag{2.13}$$

In the case of accelerated or decelerated motion ($\ddot{x} \neq 0$), the transfer load can be positive or negative. If the factors constituting N_{tr} are known, we can estimate the static axle load of the front and rear wheel. Note that in the case of acceleration and deceleration, the estimation of gross weight is assumed unchanged with and without considering the transfer load.

2.2 Static weight estimation based on averaging method

2.2.1 Axle load estimation method

The measurement devices in this study are designed for the sensor output to be insensitive to the position of the load on the loading plates. Assuming a constant speed of the vehicle passing on the loading plate, the time history of the static axle load is expressed as a rectangular function even though it will be a trapezoidal function. Considering the measurement device as a damped mass-spring model, the equation of motion in Eq. 2.14 is expressed as

$$m\ddot{z} + c\dot{z} + kz = F(t) \begin{cases} F_0, & 0 \leq t \leq \Delta t \\ 0, & t > \Delta t \end{cases} \tag{2.14}$$

where F_0 is a constant static axle load acting on the loading plate, and Δt is the duration time for the axle load to be crossing on to the loading plate.

The vibration response of the loading plate is classified into two different behaviors. One is a forced vibration response when the axle load is crossing the plate. Another is a residual-free vibration response after the axle load has finished crossing the plate. In the forced vibration response, the external force is expressed as a step function with up and down. Here, the sensor signal of the vibration response is expressed by Eq. 2.15 and depicted in Fig. 2.3.

$$y = \frac{EF_0}{k} \left[1 - \frac{e^{-\varsigma \omega_n t}}{\sqrt{1-\varsigma^2}} \cos\left(\omega_n \sqrt{1-\varsigma^2} t \right) \right] (0 \leq t < \Delta t) \tag{2.15}$$

where y is output signal from the sensor, ω_n ς and E are the natural angular frequency, the damping ratio of the loading plate's vibration and a sensor calibration factor to convert the

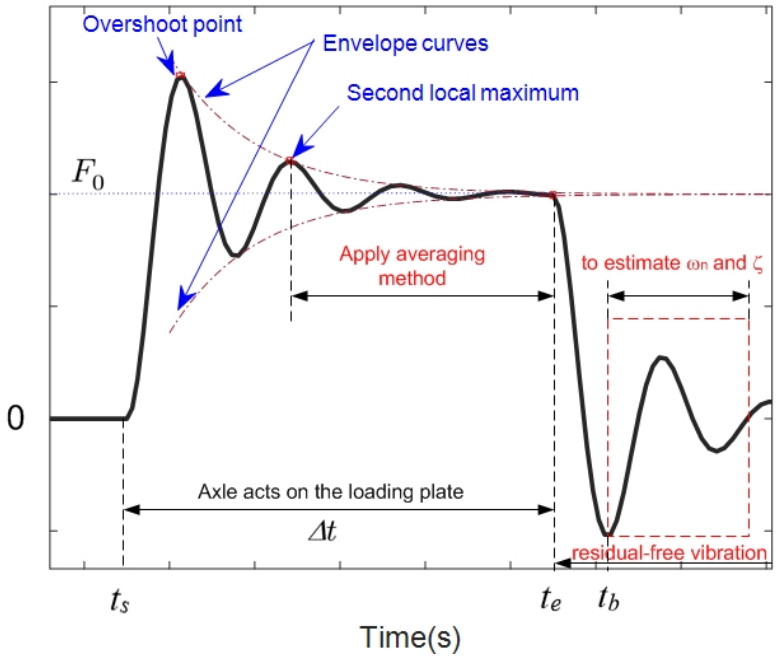

Fig. 2.3 Response function under excitation by the step function of force F_0

unit of the sensor signal to the unit "kgf" of force, respectively. The sensor signal vibrates around the static load F_0 with some degrees of attenuation as shown in Fig. 2.3. The envelope curves are expressed as the function in Eq. 2.16.

$$D(t) = \frac{EF_0}{k}\left(1 \pm \frac{e^{-\varsigma\omega_n t}}{\sqrt{1-\varsigma^2}}\right) \tag{2.16}$$

In Fig. 2.3, it is possible to identify the magnitude of the static load F_0 by means of averaging the upper and lower envelope curves from time t_s to t_b. In a similar manner, the averaging is executed for the response functions in blue but not for the envelope curves in green. It is noted that the first overshoot peak is generally much bigger than the subsequent overshoot peaks. This is because of the transient change of the external force from zero to a magnitude of F_0, as expressed in Eq. 2.14, and the damping of the vibratory system. In addition, the first overshoot is easily affected by uncertain excitation factors such as a shock generated by a wheel traveling from the end edge of the wooden runway to the front edge of the loading plate with a degree of difference in level. Therefore, the signal data in the time zone for the first overshoot should be excluded in the averaging process.

According to the simplified modeling of the contact between the tire and the ground as mentioned above, the calculation of the roll-off time t_e is performed as follows. The time t_b of the first negative overshoot point can be determined through the signal data. The time interval from t_e to t_b can be derived by solving the equation of the first derivative of Eq. 2.15 with respect to time, assuming that the initial condition is stationary.Therefore, the time interval is

$$d = t_b - t_e = \frac{1}{\omega_n \sqrt{1-\varsigma^2}} \sin^{-1}(\varsigma) \approx \frac{\pi - \varsigma}{\omega_n \sqrt{1-\varsigma^2}} \tag{2.17}$$

There is no guarantee that the initial condition is stationary in actual measurements. According to the experimental investigation of signals in this research area, it is difficult to identify the initial condition for each signal with high reliability and accuracy. Regardless, t_e is calculated by substituting into Eq. 2.17 the values of ω_n and ς obtained in advance or by curve fitting of the residual-free vibration of the signal in the dashed square shown in Fig. 2.3

2.2.2 Static weight estimation algorithm

The algorithm for the static axle load estimation of the front wheel from discretely acquired sensor signals is presented and explained in this section using Fig. 2.4. The algorithm is applicable to real-time estimation. We first assume that the unit of the output sensor signals has already been converted to weight (kgf) in the data acquisition equipment.

For convenience, the following symbols are used to specify particular points in time in the sequence of sensor signals:

$\widehat{t_k}$: time of local maxima, with k = 1, 2..., where the subscript k is the index of each local maximum point in the time series.

$\check{t}_n$: time of local minima, with n = 1, 2..., where the subscript n is the index of each local minimum point in the time series.

p_f, q_f: times when the front wheel rolls on and off the loading plate, respectively

p_r, q_r: times when the rear wheel gets on and gets off the loading plate, respectively

τ_1, τ_2: times when signals cross the threshold level in the upward and downward directions, respectively

δ: time constant of measurement device response (the second version device has $\delta \approx$ 0.015 s)

L_t: threshold level to trigger the start and stop of the recording sensor signal for estimation processing (L_t= 35 kgf in this study)

f_s: sampling rate (Hz).

$i(t_k)$: function to output the sampling index number of a signal at time t_k.

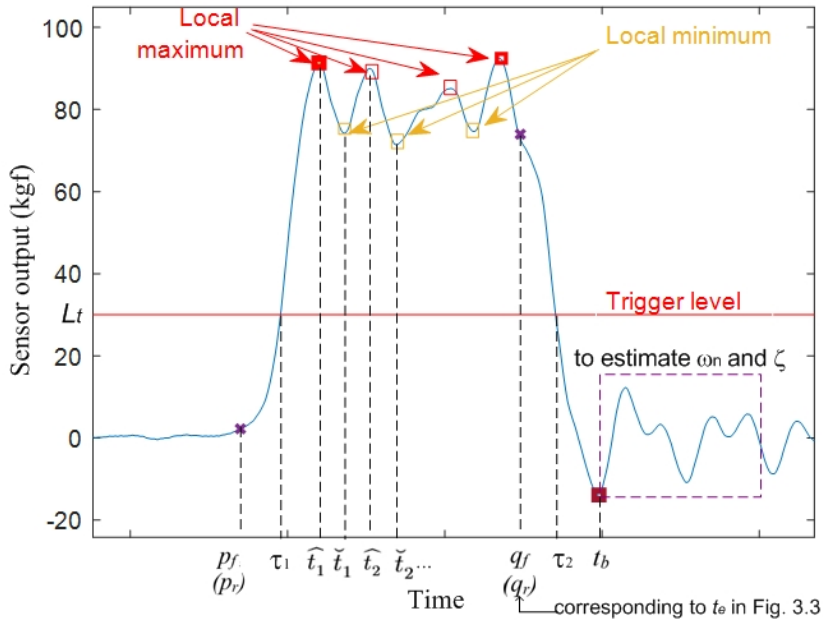

(Note: the graph line is the actual sensor signal measured in "driving mode" using PCX125)

Fig. 2.4 Schematic to explain the signal processing for averaging method

In maintaining discrete data acquisition through the moving-average filtering treatment, the estimation algorithm is composed of the following steps. We express the signal at time index t_i by $a(t_i)$.

Step 1: Find the parameters of the output signals when wheels roll on the loading plate of the measurement device.

Step 1a: Record the sensor signal from an arbitrary time instant before the starting-trigger point t_1 until an arbitrary time instant after the stopping-trigger point t_2. An example of the recorded signal using the trigger level L_t is shown in Fig. 2.4

Step 1b: Find the local maximum and minimum signals in the signal after time t_1 and before the time t_2. This is executed by checking the conditions of $a(t_i)>a(t_{i-1})$ and $a(t_i)>a(t_{i+1})$. If both these condition is true, $a(t_i)$ is recorded as a local maximum signal $a(t_k)$ (k=1, 2...). Similarly, the conditions of $a(t_i)<a(t_{i-1})$ and $a(t_i)<a(t_{i+1})$ are checked. If both these conditions are true, $a(t_i)$ is recorded as a local minimum signal $a(\check{t}_n)$ (n=1, 2...).

Step 1c: Find the time tb of the first negative local minimum signal after time t_2.

Step 1d: Identify ω_n and ς using the signal after time t_b (denoted by the dashed rectangle in Fig. 2.4). Alternatively, the parameters obtained in previous measurements and stored in the database can be used.

Step 1e: Estimate the time p_f when the front wheel rolls on the measurement device by $p_f=\widehat{t_1}-\delta$.

Step 1f: Estimate the time q_f when the front wheel rolls off the measurement device by q_f=t_b-δ.

Step 2: Apply the averaging method to the sequential signals from $a\left(\widehat{t_2}\right)$ until $a(q_f)$.

In general, the first local maximum is strongly correlated with the impulsive contact and step-function load at the moment that the wheel mounts the measurement device. The estimated normal reaction force on the front wheel, N_f, is calculated by

$$N_f = \frac{\sum_{i=i(\widehat{t_2})}^{i(q_f)} a\,(i)}{f_s\left(q_f - \widehat{t_2}\right) + 1} \tag{2.18}$$

Step 3: Estimate the normal reaction force N_r. The algorithm for the rear wheel is similar to the steps for the front wheel. The normal reaction force on the rear wheel, N_r, is obtained by

$$N_r = \frac{\sum_{i=i(\widehat{t_2})}^{i(q_r)} a\,(i)}{f_s\left(q_r - \widehat{t_2}\right) + 1} \tag{2.19}$$

where $i(q_r)$ and $i(\widehat{t_2})$ are the sampling points at time when the rear wheel dismounts the loading plate of the measurement device and the second local maximum point of the sensor signal regarding the rear wheel, respectively.

Step 4: Estimate the transfer load

Step 4a: Estimate velocity V

The velocity V is calculated approximately as the average velocity of the motorbike as it passes over the measurement device by

$$V \approx \frac{2L}{\left(p_r - p_f\right) + \left(q_r - q_f\right)} \tag{2.20}$$

where L is the wheelbase of the vehicle and a constant velocity is assumed. If the vehicle's wheelbase is unknown, the velocity can be estimated using a non-contact speedometer together with the load measurement device. Another method is to use the following formula, which considers the size of the loading plate of the measurement device in the vehicle's direction of motion (denoted by P):

$$V \approx \frac{1}{2}\left(\frac{P}{q_f - p_f} + \frac{P}{q_r - p_r}\right) \tag{2.21}$$

Step 4b: Calculate the acceleration $\ddot{x}$ to be substituted in Eq. 2.12. First, the approximate velocities of the front wheel and rear wheel (V_1 and V_2, respectively) are obtained by

$$V_1 \approx \frac{P}{q_f - p_f} \tag{2.22}$$

$$V_2 \approx \frac{P}{q_r - p_r} \tag{2.23}$$

where P is the size of the loading plate in the direction of motorbike movement. Consequently, acceleration $\ddot{x}$ is approximately calculated by

$$\ddot{x} \approx \frac{2\left(V_2 - V_1\right)}{\left(p_r - p_f\right) + \left(q_r - q_f\right)} \tag{2.24}$$

Step 4c: Estimate the transfer load N_{tr}. In this study, some parameters were numerically assumed, such as $A = 1.2m^2$, $C_L = 0.3$, $h_G/L = 0.358$, according to the reference for a typical motorbike [48] under the assumption that the center of pressure of the aerodynamic drag force coincides with the center of gravity of the motorbike, including and excluding a test driver in "driving mode" and "walking mode", respectively.

Step 11: Estimate the static axle loads, W_f and W_r, of front and rear wheel, respectively, by

$$W_f = N_f + N_{tr} \tag{2.25}$$

$$W_r = N_r - N_{tr} \tag{2.26}$$

2.2.3 Estimation method with considering underestimated results

In the first step of research, the data is processed from the second rebound top point to the end of data as mentioned at 2.2.2. However, in practice, a little under-estimation is better than overestimation for enforcement of Weigh-in-Motion. Regarding the tendency to get underestimate axle load, the estimation algorithm is developed by processing data from the first rebound bottom point after the first overshoot. Therefore, the following data sampling for averaging:

Step 1: Find the first rebound bottom point after the first overshoot.

Step 2: Find the last signal point in the period when an axle load keeps moving on the loading plate.

Step 3: Average all the signal data from the first rebound bottom point until the last signal point. The result is the estimation of the static axle load.

The dynamic load in the signal decays with some degrees due to structural damping in the measurement device, as can be seen in the schematic in Fig. 2.3. Therefore, the result in Step 3 will have a little underestimated bias theoretically. In practice, a little underestimation is better than overestimation for enforcement of WIM.

Consequently, the estimation algorithm at Section 2.2.2 is changed in data calculation of the averaging method. Apply the averaging method to the sequential signals from $a(\breve{t}_1)$ until $a(p_r)$ is applied the averaging method

$$N_f = \frac{\sum_{i=i(\breve{t}_1)}^{i(p_r)} a(i)}{f_s(p_r - \breve{t}_1) + 1} \tag{2.27}$$

The normal reaction force N_r to the rear wheel is obtained by

$$N_r = \frac{\sum_{i=(\breve{t}_1)}^{i(q_r)} a(i)}{f_s(q_r - \breve{t}_1) + 1} \tag{2.28}$$

where q_r, $\breve{t}_1$ are the time indexes when the rear wheel dismounts the loading plate of the measurement device and the first rebound bottom points of the sensor signal regarding the rear wheel, respectively.

2.3 Improvement of axle weight estimation algorithm

2.3.1 Appropriate distance between two measurement devices

An appropriate placement distance between the two measurement devices for the experiments is determined to attenuate the influence of dynamic load due to the motorbike's bounce and/or pitching mode. The right distance will enhance the accuracy of static axle load estimation. Equation (2.29) expresses the axle load downward onto the loading plate of a measurement device.

$$W = W_s + W_d \tag{2.29}$$

where W_s and W_d are static and dynamic axle loads, respectively. The measured axle load is composed of static and dynamic components. Assume that the dynamic load appears due to the motorbike's bounce and/or pitching vibration. It is expressed simply by Eq. (2.30).

$$W_d = W_0 e^{-\propto t} e^{2\pi f_n t + \varphi} \tag{2.30}$$

where W_0, f_n and $\propto$ are the amplitude, natural frequency and damping factor of the bounce and/or pitching mode respectively and φ is the initial phase.

According to the literature [48], a general motorbike has a natural frequency of bounce and/or pitching mode at a frequency from approximately 1.5 to 2.6 Hz. We conducted experiments of PCX125 with a rider seated on to find the natural frequency of bounce and/or pitching mode. It is in the range from 2.2 to 2.4 Hz. Then, we assume the general frequencies in the literature as the frequency f_n of Eq. (2.30). If the dynamic load superposes to the static load on two measurement devices that are out-of-phase mutually, the averaging method will work well to remove or reduce the influence of the dynamic load. The theoretically shortest time shift to make Eq. (2.30) mutually out-of-phase between the first and the second measurement device is expressed by Eq. (2.31).

$$\delta t \approx \frac{1}{2f_n} \tag{2.31}$$

In our experiment, when a test motorbike runs at a speed of approximately 40 km/h (V=11.1 m/s), the placement distance between two devices is calculated as in Eq. (2.32).

$$D = V\delta t = \frac{V}{2f_n} \approx 2.1 \ \ to \ 3.7 \ (m) \tag{2.32}$$

where D is the distance between the centers of the two devices. Therefore, the placement distance of the two measurement devices is set as 2.3 m in our experiment. In case of very slow speed, this distance will not be important because the dynamic load will become weak.

2.3.2 Estimation of Speed and Acceleration/Deceleration Using Two Loading Plates

Various sensing systems are available today to measure or estimate vehicle speed and acceleration rate from a stationary point on the ground such as radar Doppler system or inductive loop detector system. In this research, we present another method using the sensor signal from two measurement devices of WIM. It is efficient to use the devices for not only weighing but also sensing vehicle speed and acceleration.

As shown in Fig. 2.5, let us place two identical measurement devices, with a distance of D between the front edges of two loading plates. The moments the front wheel of the motorbike gets on the loading plates of the two devices are denoted by t_{f1} and t_{f2} and for the rear wheel by t_{r1} and t_{r2} (as can be seen in Fig. 2.6). The average speed during which the front wheel moves from the front edge of the first measurement device to that of the second one is calculated by Eq. (2.33). Let us assume that the speed is the instant speed at time of $\frac{t_{f1}+t_{f2}}{2}$ for the front wheel. The average speed during which the rear wheel travels from the front edge of the first measurement device to that of the second one is calculated by Eq.(2.34).

Let us assume that the speed is the instantaneous speed at time $\frac{t_{r1}+t_{r2}}{2}$ for the rear wheel. Consequently, the acceleration is obtained as the increment rate of speed in the period from $\frac{t_{f1}+t_{f2}}{2}$ to $\frac{t_{r1}+t_{r2}}{2}$ by Eq. (2.35).

$$v_1 = \frac{D}{t_{f2} - t_{f1}} \tag{2.33}$$

$$v_2 = \frac{D}{t_{r2} - t_{r1}} \tag{2.34}$$

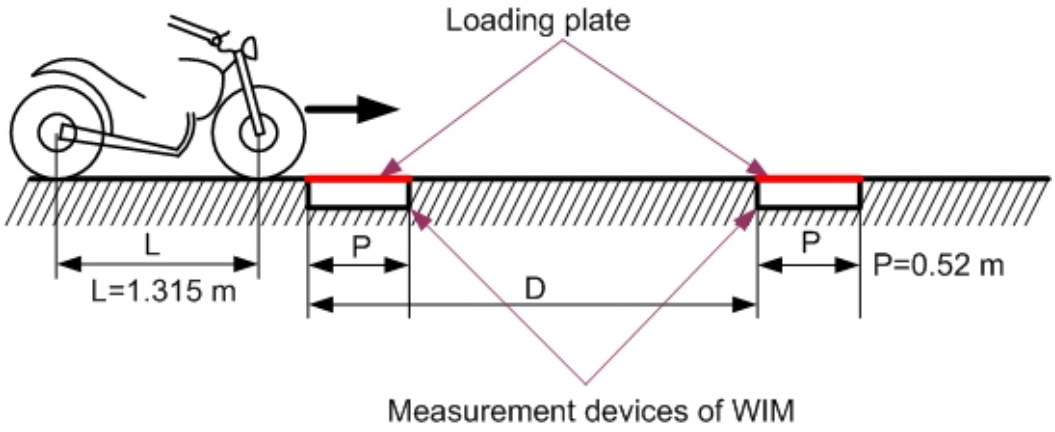

Fig. 2.5 Schematic of experimental setup and placement

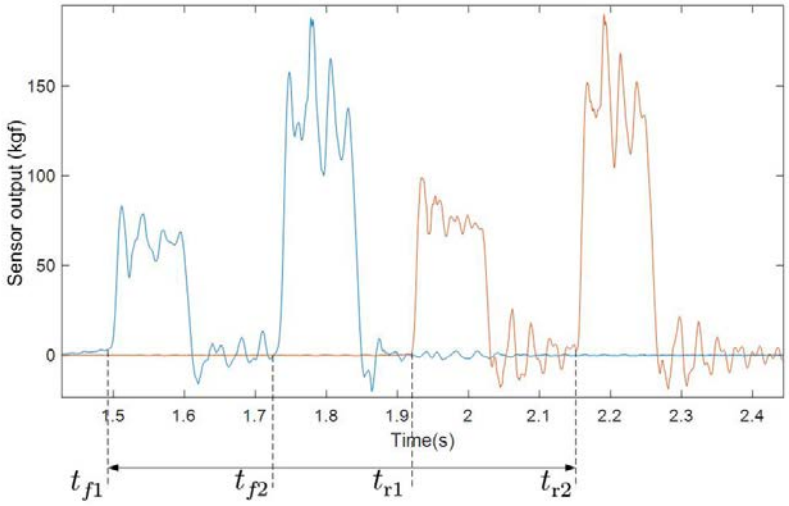

Fig. 2.6 Time detections in a real output signal

$$a = \frac{2\,(v_2 - v_1)}{(t_{r1} + t_{r2}) - (t_{f1} + t_{f2})} \tag{2.35}$$

$$\bar{v} = \frac{v_1 + v_2}{2} \tag{2.36}$$

Even when using the sensor signal, it is not easy to pinpoint the exact time at which a wheel gets on and off a loading plate. Nevertheless, the estimation of the moment a wheel gets on is more reliable than the moment it gets off because the first overshoot peak can be clearly pointed out. In Section 2.2.2, I proposed an estimation algorithm to determine the moment a wheel gets on and off a loading plate from the first overshoot point and the first rebound bottom point of the sensor signal. The calculation is done after the plate is released from the axle load using the time constant of the measurement device's dynamics. I propose an improvement of the estimation of the duration a wheel travels from the front edge of the first plate to that of the second one, as shown in Fig. 2.5, by using the first overshoot points in the sensor signal at the moment a wheel just gets on two loading plates. The time of getting off the loading plates is not utilized.

Let us denote the time constant from the time a wheel gets on a loading plate to the first overshoot point by c. The times t_{f1} and t_{f2} at the moment the front wheel gets on the first and the second loading plate are estimated by $(\hat{t}_{f1} - c + \varepsilon_1)$ and $(\hat{t}_{f2} - c + \varepsilon_2)$ respectively. Here, $\hat{t}_{f1}$ and $\hat{t}_{f2}$ are the times of the first overshoot points in the sensor signal from the first and the second loading plates, and ε_1 and ε_2 are inaccuracy quantities in estimation respectively. The following equations are obtained as following

$$t_{f2} - t_{f1} = \left(\hat{t}_{f2} - c + \varepsilon_2\right) - \left(\hat{t}_{f1} - c + \varepsilon_1\right) = \hat{t}_{f2} - \hat{t}_{f1} + \varepsilon_2 - \varepsilon_1 \tag{2.37}$$

where $(\varepsilon_2 - \varepsilon_1)$ can be expected to be much less than ε_1 and ε_2 because ε_1 and ε_2 are considered almost same quantities. In the same way, the following equations are obtained

$$t_{r2} - t_{r1} = (\hat{t}_{r2} - c + \varepsilon_2\ ) - (\hat{t}_{r1} - c + \varepsilon_1) = \hat{t}_{r2} - \hat{t}_{r1} + \varepsilon_2 - \varepsilon_1 \tag{2.38}$$

for the rear wheel's movement. Eventually, the denominator of the fraction to estimate the acceleration in Eq. (2.35) becomes free from inaccuracy quantities because

$$(t_{r1}+t_{r2})-(t_{f1}+t_{f2}) = (\hat{t}_{r1}+\hat{t}_{r1}) - \left(\hat{t}_{f1}+\hat{t}_{f1}\right) \tag{2.39}$$

The first overshoot point will be pointed out clearly in most cases. Namely, Eq. (2.35) is obtained by

$$a = \frac{2\,(v_2 - v_1)}{(\hat{t}_{r1}+\hat{t}_{r1}) - \left(\hat{t}_{f1}+\hat{t}_{f1}\right)} \tag{2.40}$$

In the section 2.2.2, using a single loading plate, the time a wheel just gets on and off a loading plate is estimated by $\hat{t}_{f1} - c + \varepsilon_1$ and $\hat{t}_{fb} - c + \varepsilon_b$. Here, $\hat{t}_{fb}$ and ε_b are the time of the first rebound bottom point after the wheel gets off the loading plate and an inaccurate quantity respectively. Note that ε_b is considered bigger than ε_1 because of the big dynamic load's inclination, with some uncertainties toward the sensor signal. The duration time Δt of a wheel crossing on the loading plate is calculated as

$$\Delta t = (\hat{t}_{fb} - c + \varepsilon_b) - (\hat{t}_{f1} - c + \varepsilon_1) = \hat{t}_{fb} - \hat{t}_{f1} + \varepsilon_b - \varepsilon_1 \tag{2.41}$$

The Δt will be worse in accuracy than the above mentioned algorithm.

2.3.3 Estimation of transfer load between front and rear wheels

The transfer load is calculated by

$$\Delta N = \frac{h_G}{L} ma \tag{2.42}$$

where L, h_G, m are the vehicle's wheelbase, the height of the center of gravity and the mass of the vehicle respectively, and a is acceleration. As mention in Section 2.1, in case of speed smaller than 40 km/h, the aerodynamic draft is too small compared to the weight of motorbike, so it is ignored in the equation.

The method in Section 2.3.2 has potential to estimate more accurate acceleration than the method in Section 2.2.2 using a single measurement device. However, note that the wheelbase and the height of the center of gravity of vehicle are necessary to calculate the transfer load. The static axle loads of the front and the rear wheel with consideration of the transfer load are obtained by

$$W_f = N_f + N_{tr} \tag{2.43}$$

$$W_r = N_r - N_{tr} \tag{2.44}$$

where N_f and N_r are the measured axle loads about the front and the rear wheel, and N_{tr} is the transfer load calculated by Eq. (2.42).

In this study, the wheelbase L is known as L=1.315 m in the specification of the motorbike. However, the exact height, h_G, of the center of gravity of the motorbike in moving condition with a seated rider is difficult to measure. The test rider's weight is approximately 77 kg, and the weight of the motorbike is approximately 132 kg.

A ready reference [48] reports that the ratio of the height, h, of the center of gravity above the ground for a general motorbike without a rider, with respect to the wheelbase L, is approximately 0.3 to 0.4. The wheelbase L of the test motorbike in this study is approximately 1.315 m. Therefore, the height of the center of gravity is calculated as $h \approx 0.52$ m. The height of the mass center of the test rider seated on the motorbike is assumed at approximately 1.1 m above the ground. As a result, the height of the center of gravity from the ground of the test motorbike, including a test rider, in running conditions is assumed as 0.74 m.

2.4 Estimation algorithm for a light truck

As mentioned in Section 3.1, the experiments with a light truck are conducted independently both left and right sides. Due to the configuration of the measurement device, the load estimation algorithm for the wheels of the truck is similar to motorcycles in Section 2.2.

In this study, the center of gravity of the truck with a driver is assumed with the height 0.9 meter from the ground. According to the specifications of the Sambar truck [49], the radius of the wheel is 0.297 meter and the wheelbase is 1.9 meter. Therefore, the $h_G/L = 0.32$.

Chapter 3

Measurement device and experimental setup

3.1 Measurement devices

One of the big challenges for the WIM study in university is the design of a measurement device and experimental course conditions because of some factors such as cost, time and the size of the measurement device. Considering the essential point at the preliminary stage is to focus on the critical factors to be clarified, a miniature WIM system was constructed for a motorbike to conduct an experimental investigation. The benefit of using a miniature system is low-cost, time-saving, and compact as well as an easy arrangement of the experimental course. The results will be applicable for the development of another device for a light truck at the next stage, and a full-scale system in the future. In addition, the research of the WIM for a motorbike in motion is more interesting from an academic viewpoint because of factors such as driver behavior, steering characteristics, and bike-body behavior in accelerating and decelerating modes. These factors will change the front and rear load more significantly on a motorbike than on trucks or cars.

In the initial stage, the requirements of a miniature measurement device for experiment with a motorbike (Table 3.1). According to the general size of plate-type measurement devices for a truck, as shown in Section 1 (Figs 1.14 and 1.15), the length of a loading plate in traveling direction is required to be smaller than 90 cm to avoid the influence of signal interference of two wheels. Based on the requirements, two kinds of measurement devices suitable for motorbikes were designed as a result of basic experimental research on WIM. In the next step, based on the results obtained from experiments with motorbikes, a measurement device for a light truck is developed. Compared to motorbikes, to measure

Table 3.1 The requirement of a miniature device with a motorbikes

Size	Loading plate: $\leq$ 90 cm
The capacity of measured load	1$\sim$200 kgf
Vehicle Speed	0 $\sim$50 km/h
Others	- Minimize the impact factors due to shock vibration - Independent on vertical force position - High-signal-noise ratio, damping ratio.

the axle weight of truck, the WIM system needs to measure two sides of a truck while it is crossing the measurement device. It means the measurement device must measure the left and right side of the wheels of the trucks. There are two types of measurement configuration for that requirement. The first option is the measurement device has the width, which is larger than the track width of the truck (Fig. 3.1). Another option is two independent parallel measurement devices measuring two wheels at the same time (Fig. 3.2). The option using two independent parallel devices are chosen due to considering the factors such as economy, maximum load capacity of equipment, and road construction. Two separate devices will obtain the results, and the axle weight will be calculated as the total estimated load from each measurement device. Consequently, the experiments for a truck need only a measurement device in consideration of road construction. The experiments are conducted both left and right sides independently. A scale measured the static load of the front and rear wheels on both sides (left and right). These results of static weight are used as references to the estimation results. The requirements of a measurement device for experiment with a light truck are in Table 3.2.

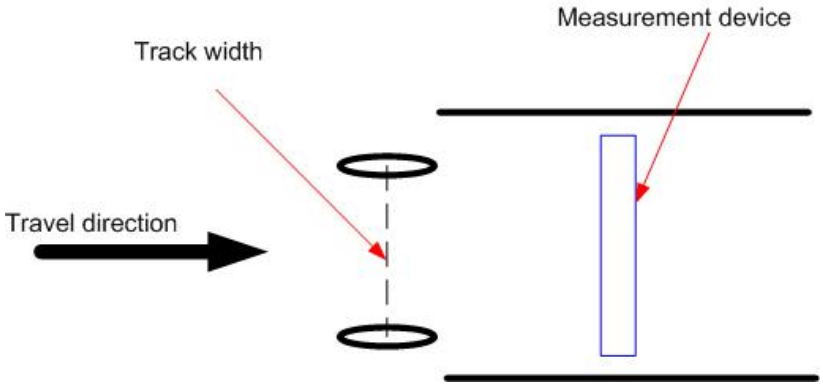

Fig. 3.1 First configuration of WIM for truck

Table 3.2 The requirement of a miniature device with a light truck

Size	Loading plate: $\leq$ 90 cm
The capacity of measured load	1$\sim$300 kgf
Vehicle Speed	0 $\sim$50 km/h
Others	- Minimize the impact factors due to shock vibration - Independent on vertical force position - High signal noise ratio, damping ratio.

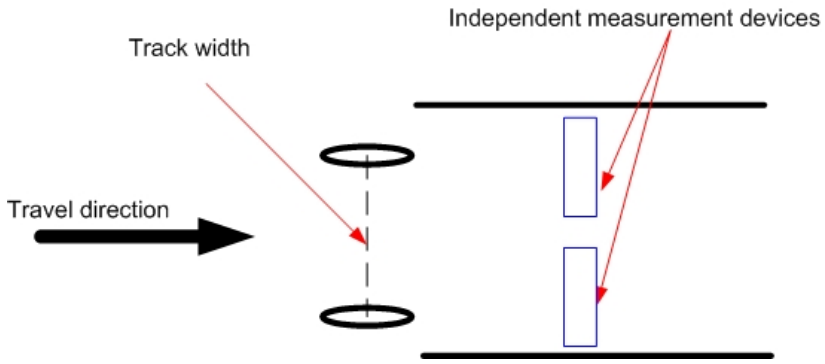

Fig. 3.2 Second configuration of WIM for truck

3.1.1 First version of measurement device for motorbikes

The first version was built based on a lever-type of scale mechanism manufactured by Tanaka company (weighing capacity of 200kgf). The design concept of the measurement mechanism is shown in Fig. 3.3. The system has the loading plate, denoted by EF, which is supported on the lever mechanism. The measurement system is designed with a compact size, and all lever parts are considered to behave as rigid bodies. The external load and its position are expressed by f and x, respectively. According to the geometry, the force, F_s, acting at the elastically tension spring GH is obtained as

$$F_S = \frac{F}{L_B}\left\{L_1 + \left(L_2\frac{L_3}{L_C}\frac{1}{L_P} - \frac{L_1}{L_P}\right)x\right\} \tag{3.1}$$

Therefore, if the lever size constraint is designed as Eq.3.2, the force Fs becomes independent from the external load position x, and is expressed by Eq.3.3.

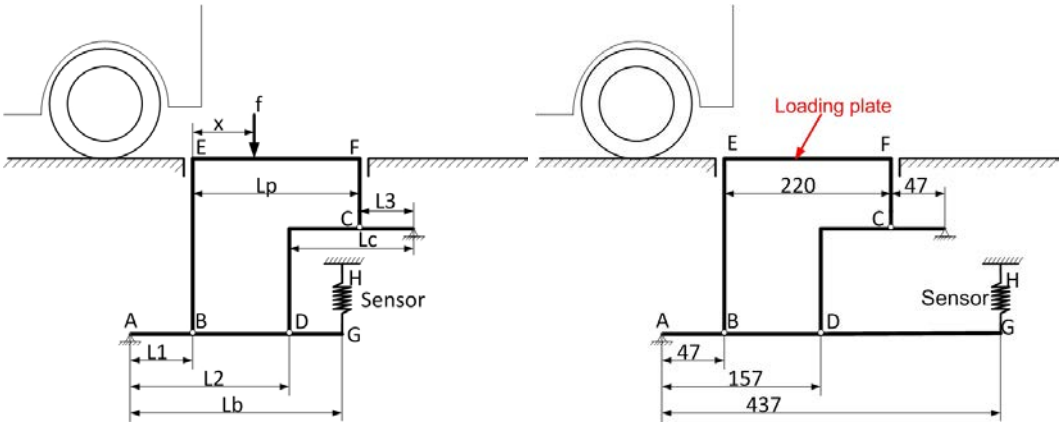

(a) Force acting on the loading plate (b) Actual size

Fig. 3.3 2-D schematic of lever mechanism

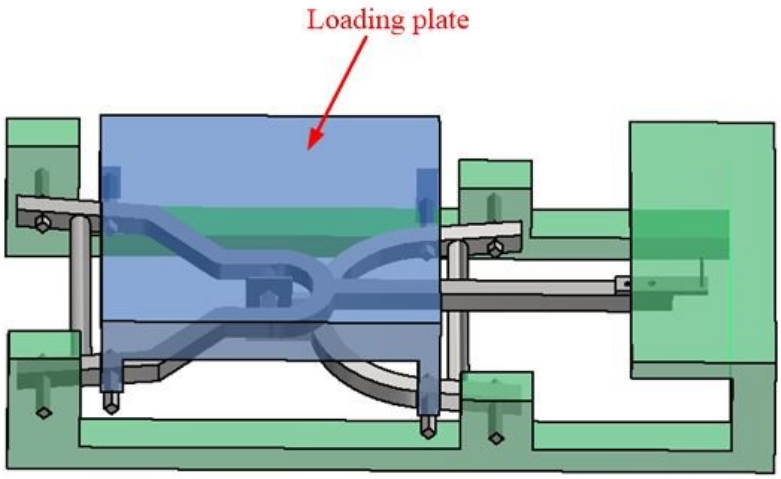

Fig. 3.4 3-D schematic of measurement device

$$L_1 = \frac{L_2 L_3}{L_C} \tag{3.2}$$

$$F_S = \frac{F L_1}{L_B} \tag{3.3}$$

The lever mechanism was designed to realize load-position-independent measurements, which means that the load sensor's output is insensitive to the placement of a particular weight at any position on the loading plate. The length of the size of the loading plate is 220 mm in the motorbike's passing direction. All lever parts are considered to behave as rigid bodies, while the load sensor is a Kyowa strain gauge (Fig. 3.4). A steel plate with length and width are the same as loading plate and thickness 20 mm was put on a miniature device to ensure its durability of dynamic force. The natural frequency of measurement device is approximately 27 Hz.

However, the author experimentally found some problems with the device such as low damping ratio, as shown in Fig. 3.11a. The output signal sometimes has a non-zero balance phenomenon after each trial (Fig. 3.5) due to the design of mechanism and sensor. Moreover, when the speed of the motorbike exceeds 16 km/h, the device cannot acquire a sensor signal during a longer time period than a single period of the device's first natural vibration because of the size of the loading plate.

3.1.2 Second version of measurement device for motorbikes

The second version has been developed based on a commercial weighing scale Ohaus ES, which uses four load cells at the four corners under the loading plate. Each load cell is composed of a small cantilever and four strain gauges connected in the form of the Wheatstone bridge circuit, and works as a single-point load sensor in the vertical direction. The total output signal (voltage) from four load cells is converted to the value of applying load. The loading plate can be assumed to behave a rigid plate within the load range up to approximately 200kgf. Then, the resultant output realizes the insensitivity of loading position on the loading plate. The size of the loading plate is 400 x 520 mm where the 520 mm side is in the vehicle's running direction. Compared to the first version with lever mechanism configuration, the second version has more advantages, such as higher linearity, damping ratio, signal-noise-ratio, and no non-zero balance phenomenon (Table 3.3). Because a load cell is designed with four strain gauges, it has higher linearity, damping-ratio (Fig. 3.10b, Fig.

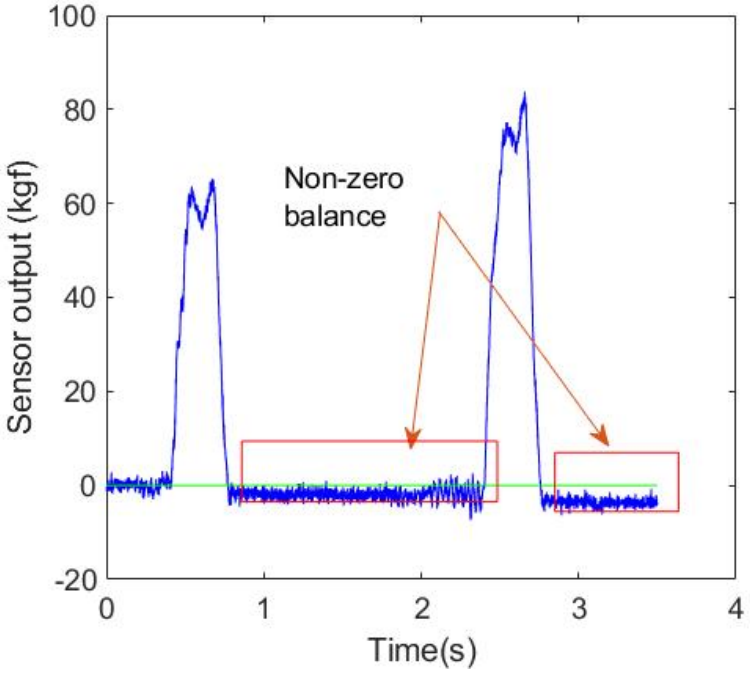

Fig. 3.5 Non-zero balance phenomenon of first version after each experiment

3.11b). In addition, because the measurement device is connected to the same ground with the data acquisition system, the signal-noise-ratio signal of the second measurement device is much higher than the first version. The natural frequency of the measurement device is approximately 35 Hz.

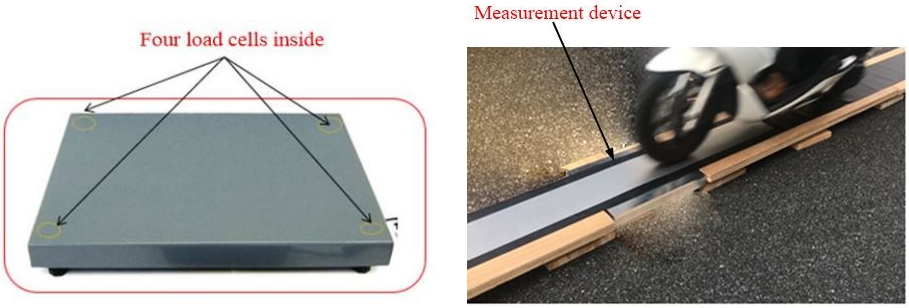

(a) Front view of measurement device (b) Actual experiment

Fig. 3.6 Second version of the miniature measurement device

Table 3.3 General comparison between first and second measurement device

	First version	Second version
Size of loading plate	22 cm	52 cm
Linearity	RMSE: 1.939	RMSE: 0.0104
Damping ratio	Low	High
Noise	± 4kg	±0.5 kg
Non-zero balance	Sometimes	No

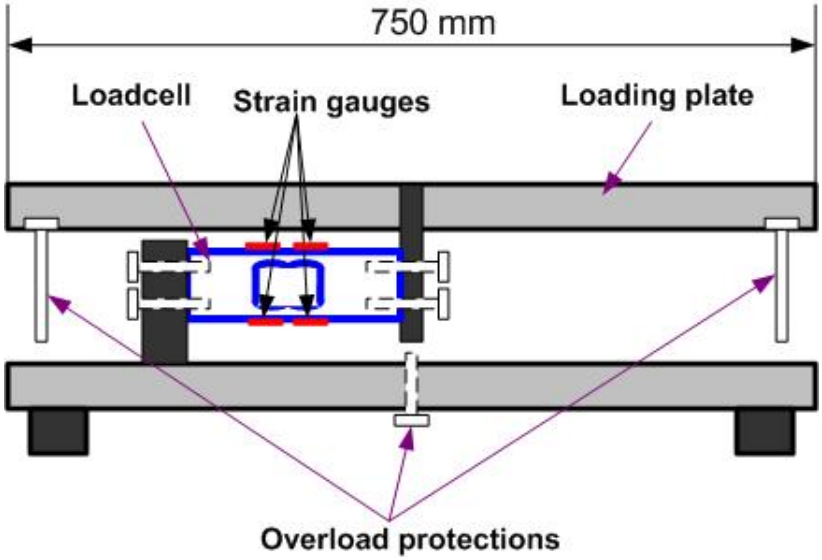

Fig. 3.7 A measurement device for truck test

3.1.3 Measurement device for a light truck

Based on the knowledge obtained from the experiments with miniature devices, a measurement device for a light truck is developed. Because the requirement of a wheel load of a light truck is 300 kgf, a commercial weighing scale Yamamoto DP is selected. The size of the loading plate is 750x500 mm (Fig. 3.7). The natural frequencies of the measurement device are approximately 25 Hz and 45 Hz. The measurement device is also designed with a single point load cell (or platform load cell).

Assuming that the external load and its position are expressed by F and x, respectively (Fig. 3.8). Considering the measurement device is designed to behave as rigid bodies. According to the geometry, the force, F and the moment M act at position a and b is obtained as

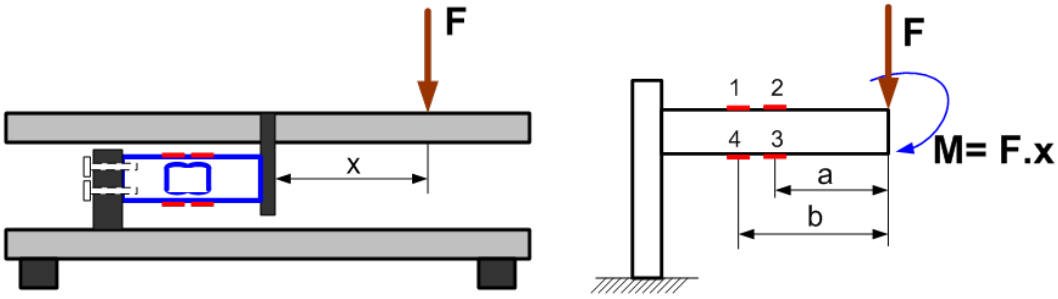

(a) Force F acting on the loading plate (b) Load cell as a cantilever

Fig. 3.8 Force acting on the measurement device

$$M_a = aF + M \tag{3.4}$$

$$M_b = bF + M \tag{3.5}$$

$$M = xF \tag{3.6}$$

Strain gauges are connected by the configuration of the Wheatstone bridge circuit, the voltage output as below [50]

$$output = \frac{k_G}{4}(\varepsilon_1 - \varepsilon_2 + \varepsilon_3 - \varepsilon_4)E \tag{3.7}$$

where k_G is gauge factor, ε is strain, E is Young's modulus.

Because a, b are constants and the moment M from Eqs.3.4 and 3.5 is not exist after the subtraction (Eq. 3.7), the output is insensitive with the position of force.

3.2 Data acquisition and calibration

Sensors (a strain gauge in the first version or load cells in the second version) in measurement devices are connected to the data acquisition system (Graphtec GL7000)(Fig. 3.9). The signals are finally sent to a computer and are analyzed to estimate the static load. In order to

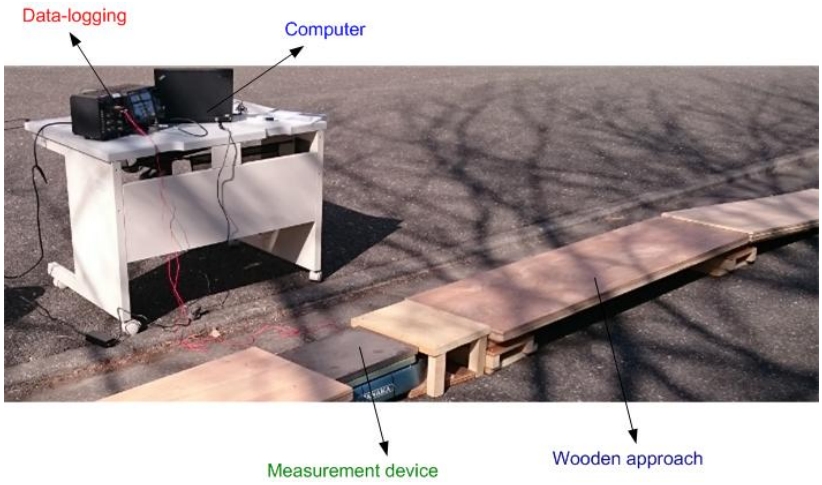

Fig. 3.9 Experimental setup

deal with noise, the sensors are connected to the ground. Because the time for motorbike passing the measurement device is very short, the data logging system is set up with a high sampling rate 2kHz. Before conducting experiments, the measurement devices were calibrated with the known weights by using the least square algorithm (Fig. 3.10).

Figure 3.11a is an example of the sensor signal actually obtained using the first-version device. Figure 3.11b is the signal obtained by the second-version device. The second miniature device has advantages compared to the first-version device. This second version has a much higher damping ratio and linearity. The signal-to-noise ratio is also higher than the first one. There are two main reasons for this result. Firstly, because the measurement device is connected to the same ground with the data acquisition system, so it cancels the noise from the power supply. Secondly, the strain gauges in the load cells are connected in the Wheatstone bridge circuit, the white noise of one sensor is reduced. In addition, the size-up of the loading plate realizes the sensor signal acquisition of more than one period of the first natural vibration of the device for motorbike speeds of up to 40 km/h. Therefore, the experiments data for motorbikes in the following chapter were performed on the second version.

Figure 3.12 shows the calibration procedure and sensor output for a trial of a light truck. As can be shown from the figures, the measurement device has a high linearity, damping ratio and low noise.

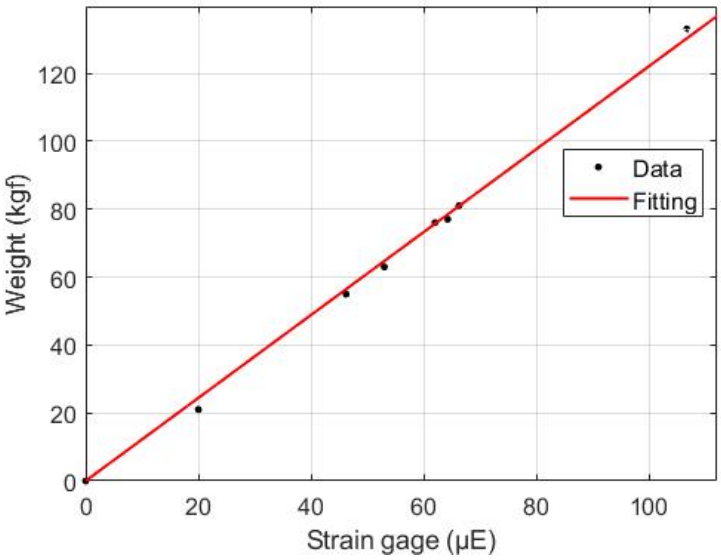

(a) First version measurement device

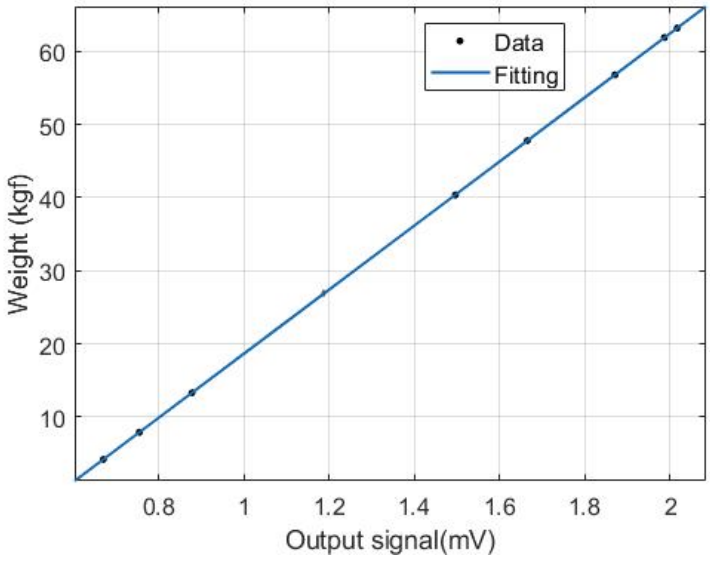

(b) Second version measurement device

Fig. 3.10 Calibration procedure

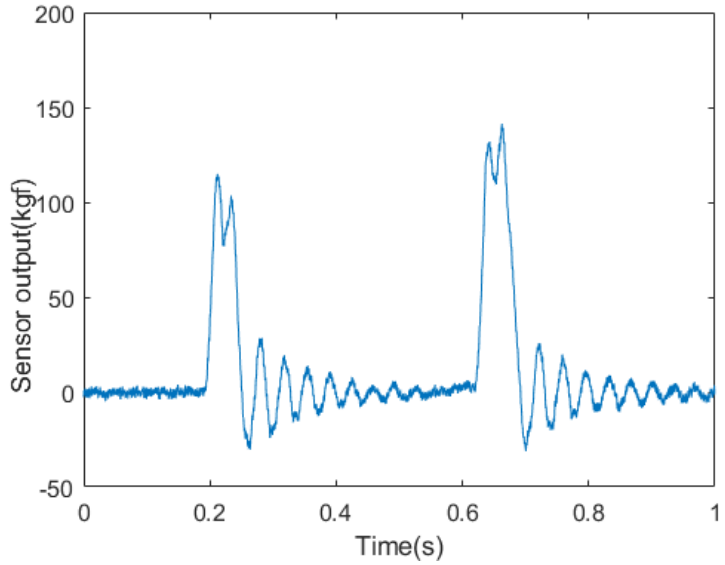

(a) Using the first-version device (V=14.3 km/h)

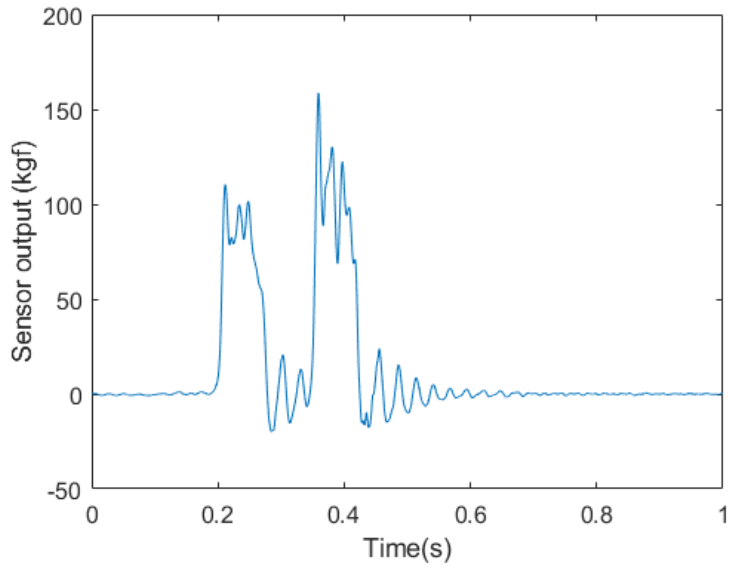

(b) Using the second-version device (V=26.5 km/h)

Fig. 3.11 Examples of sensor signals of the first and second versions of the measurement device (one test motorbike)

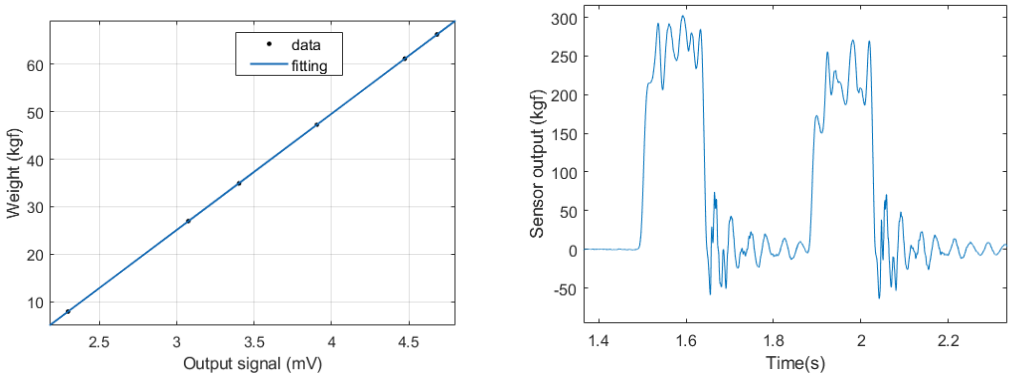

(a) The calibration procedure (b) Sensor output for a trial

Fig. 3.12 A measurement device for a light truck

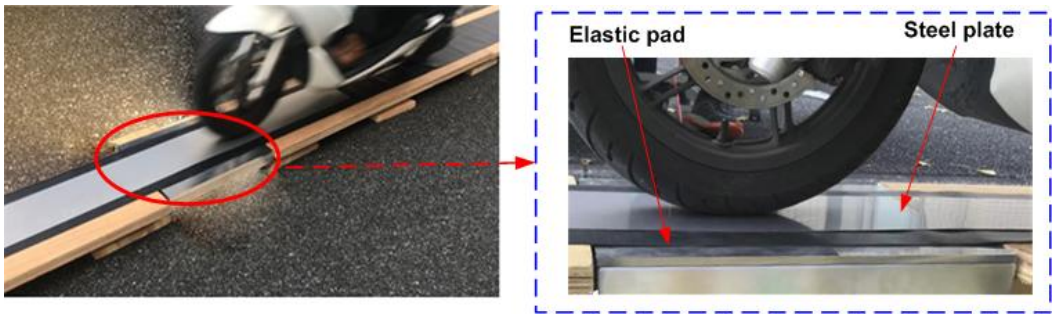

Fig. 3.13 An elastic pad and a steel plate

3.3 Experimental setup

3.3.1 Experiments with motorbikes

The experiments were carried out on the paved ground in Tokyo Tech's campus (See at Appendix A). Initially, since the ground cannot be dug, the measurement device was placed on the ground together with the wooden runway for a test motorbike to move on, as shown in Fig. 3.13. A thin elastic pad and a thin steel plate with a thickness of 1 mm were layered on the device and the wooden runway from one side to the other. The purpose of the layering is to weaken the impulsive vibration just at the moment when a test motorbike runs onto the loading plate of the device from the wooden runway. The measurement system consists of the measurement device and a computer for data acquisition and analysis.

Fig. 3.14 Ensuring safety after experiments

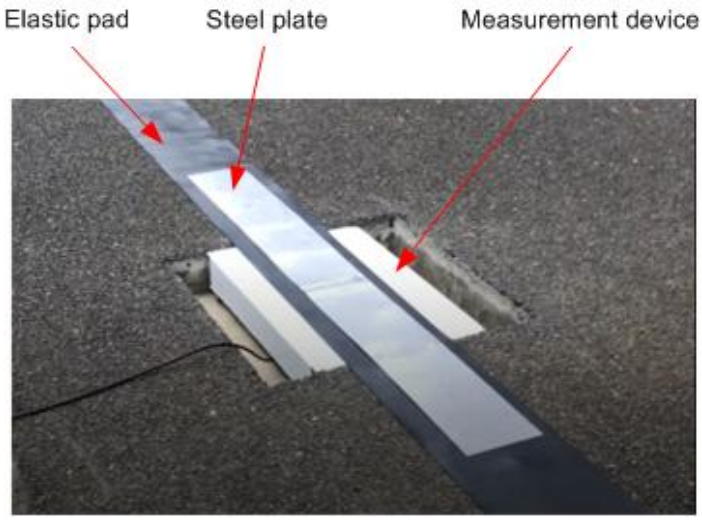

Fig. 3.15 Set up experiment for a truck

3.3.2 Experiments with a light truck

In the preparation of experiments with a light truck, we constructed the road in Tokyo Tech campus. Next, we set up the measurement device with almost the same level as the road. A barrier and warning signs are installed to ensure safety for drivers and pedestrians on the campus after experiments (Fig. 3.14). To minimize the shock vibration problems when trucks passing the measurement device in the tests, an elastic pad and thin steel plates are also used as in the experiments of motorbikes (Fig. 3.15).

Chapter 4

Experiments and results

The experiments were conducted in Tokyo Tech's campus. While the experiments with motorbikes is conducted mainly with PCX125, the experiments with a truck is performed with a light truck Sambar.

Accuracy evaluation

The accuracy of the estimated axle loads, and gross weights of the motorbikes are investigated in this study by means of calculating the estimation error, defined by

$$\frac{W - W_s}{W_s} \times 100\% \tag{4.1}$$

where W and W_s are the estimation result and true static axle load, respectively.

4.1 Experiments with a single measurement device for motorbikes

The experiments were performed at a variety of speeds and two moving modes of the motorbike - "walking mode" and "driving mode" (Fig. 4.1). In "walking mode" a motorbike passed the measurement device while being pushed forward by a walking person. In "driving mode" a motorbike passed the measurement device under engine power with a person riding. Thus, the static load of each wheel in "walking mode" excludes the person's weight, while the person's weight is included in "driving mode". In this section, the experiments with two versions of miniature devices is presented.

Note that the estimation results in this section are calculated based on the algorithm presented in Section 2.2.2.

(a) Walking mode (b) Driving mode

Fig. 4.1 Experiment with the motorbikes

4.1.1 First version miniature device

Table 4.1 shows the static axle loads of the test motorbike PCX 125 in the "walking mode" and "driving mode". The weights are measured in the stationary condition using a digital platform scale on the site prior to the experiment of WIM. It is verified that the static axle loads vary about ±4 kgf from the values of "driving mode" in Table 4.1. The fluctuation of ±4 kgf is observed by depending on changing the rider's body posture forward and backward on the seat.

Table 4.1 The weight of the motorbike including driver by stationary weighing

Mode	Front load (kgf)	Rear load (kgf)	Gross weight (kgf)
Walking	54.9	81.6	136.5
Driving	76	132	208

Note: the measurement varies about ±4 kgf depending on changing the rider's body posture forward and backward on the seat (driving mode).

Table 4.2 The estimation results in the "walking mode" using PCX125

No	Velocity (km/h)	Front load (kgf)	Front error (%)	Rear load (kgf)	Rear error (%)	Gross weight (kgf)	Gross error (%)
Trial 1	2.3	57.6	4.9	72.7	-10.9	130.3	-4.5
Trial 2	2.3	56.2	2.3	74.9	-8.2	131.1	-4
Trial 3	2.35	56.1	2.1	75.6	-7.3	131.7	-3.5
Trial 4	2.4	57.9	5.4	73.7	-9.7	131.5	-3.7

Note: Errors in three columns are calculated using the values in Table 4.1 for W_s by Eq. (4.1)).

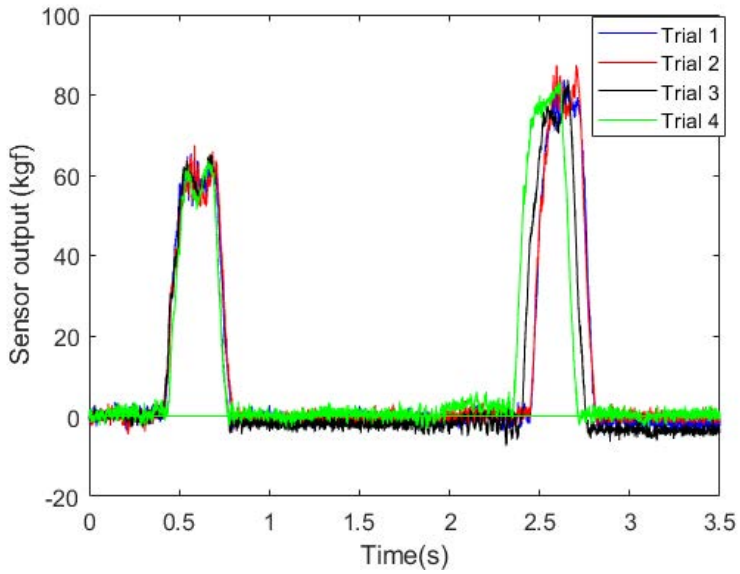

Fig. 4.2 Experiment data in “walking mode” at almost same speeds
(data1:2.3 km/h; data2: 2.3km/h; data3: 2.35km/h; data4: 2.4km/h)

Figure 4.2 shows four experimental data in “walking mode”. The speeds of motorbike are not so different among four experimental trials. The true static axle loads of the front and the rear are 54.9kg and 81.6 kg, respectively. Since the speed of motorbike moving on the loading plate, whose size is 22 cm is comparatively very lower than “driving mode”, the duration time in which an axle load moving on the loading plate becomes long enough to apply the averaging method. Note that, the measurement device has a high signal noise, the average moving filter is used to filter the sensor output signal before applying the estimation algorithm. Table 4.2 presents the errors of the static load estimations in "waking mode". The estimation results are acceptable accuracy. The estimation errors of gross weight are less than 5% (4/4 trials). The estimation errors of wheel loads are less than 10% (7/8 cases).

However, experiments with the velocity higher than 16 km/h, it is impossible to apply the averaging method because the signal output has only one peak. Figure 4.3 shows experimental data with velocity about 20 km/h. In addition, this device also had a problem of non-zero balance after motorbike getting off the device (Fig. 4.4). That means, the signal sometimes cannot come back to zero condition after motorbikes getting off the device. Thus, the zero-balance calibration needed to do before each trial.

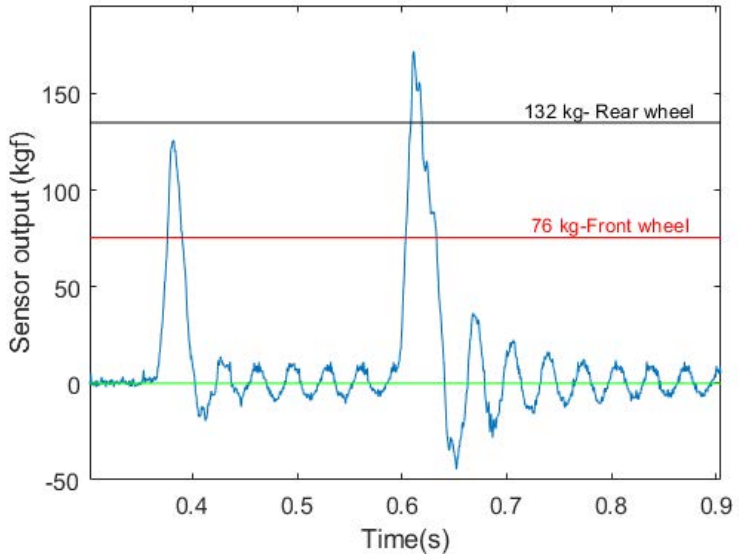

Fig. 4.3 Experiment data in “driving mode” with speed 20 km/h

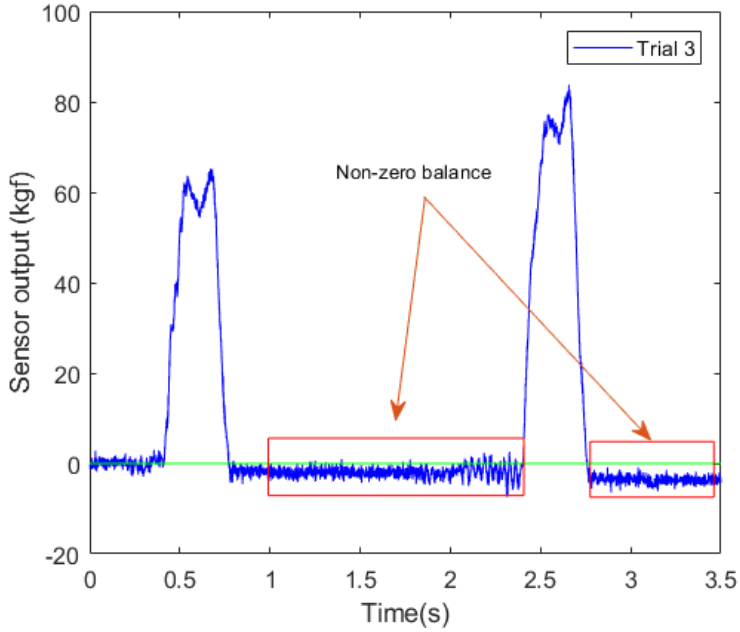

Fig. 4.4 Problem of non-zero balance

4.1.2 Second version miniature device

Figure 4.5 shows the three motorbikes used for experiments with the second version miniature device. Table 4.3 shows their static weights, including the weight of the seated rider, measured using a digital platform scale on the site prior to the experiments. Each motorbike was driven by a different person.

(a) PCX125 (b) CBR1100 (c) XR250

Fig. 4.5 Three types of motorbikes used for experiments

Table 4.3 The weight of the motorbike including the rider measured on the site of experiments

Model of motorbike	Front load (kgf)	Rear load (kgf)	Gross weight (kgf)
PCX125	78.8	125.1	203.9
CBR1100	149.5	168.3	317.8
XR250	85.9	101.5	187.4

Note: including the weight of rider on seat

"Walking mode"

Figure 4.6 shows the sensor signal data of experiments at four different speeds in "walking mode" using PCX125. Table 4.4 shows the estimation results from the data. As can be seen in the table, the estimation results have small errors, less than 5%. In addition, most of the results were underestimated.

Driving mode with almost constant speed

The experiments of "driving mode" were conducted using three types of motorbikes. The true static weights of motorbikes (Table 4.3) with a driver are measured before the experiments. Figure 4.7 shows the sensor signal data of experiments at four different speeds in "driving mode" using PCX125. Table 4.5 shows the estimated axle load and gross weight from the

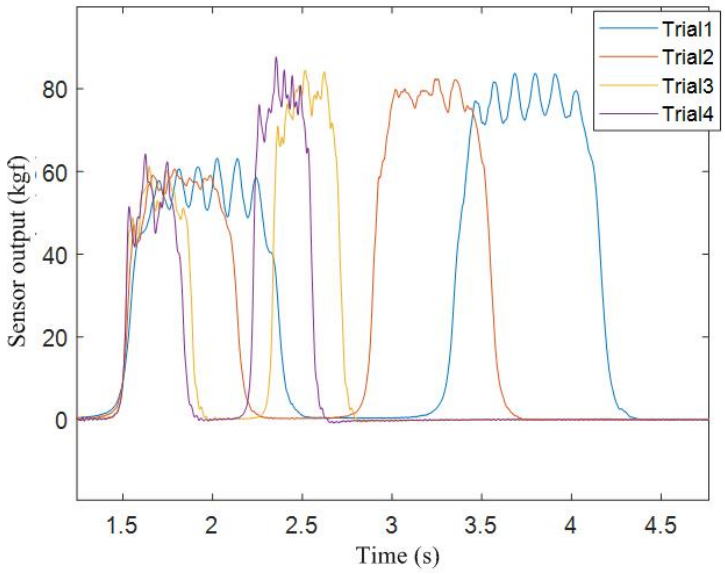

Fig. 4.6 Sensor outputs in “walking mode” with PCX125

Table 4.4 The estimation results in the “walking mode” using PCX125

No	Velocity (km/h)	Front load (kgf)	Front error (%)	Rear load (kgf)	Rear error (%)	Gross weight (kgf)	Gross error (%)
Trial 1	2.3	54.0	-1.2	76.6	-2.5	130.6	-2.0
Trial 2	2.9	55.1	0.6	76.1	-3.0	131.2	-1.5
Trial 3	4.9	52.7	-3.6	76.9	-2.1	129.6	-2.7
Trial 4	5.7	52.1	-4.8	76.3	-2.8	128.3	-3.6

Note: True axle load of the front wheel is 54.7 kg, and that of the rear wheel is 78.5 kg.

signal data. Tables 4.6 and 4.7 present the estimation results for the use of CBR1100 and XR250, respectively. It is noted that most of the results are underestimated. The estimation of the axle loads was slightly worse than those of "walking mode". One possible reason is that motorbikes did not run at precisely constant speeds. Another reason is that the test rider's posture including seat positioning may have been different and may vary with some degree at all trials. It is also different from those from the static measurement of the data shown in Table 4.3. In fact, it was verified that the static axle loads varied by approximately ±4 kgf when the author carried out experiments by changing the upper half of rider's body posture forward and backward on the seat by intention in the measurement for the data shown in Table 4.3. Note that the test riders are not professional riders. Nevertheless, as can be seen in Tables 4.5, 4.6, and 4.7, all four estimations of gross weight were obtained with practical accuracy.

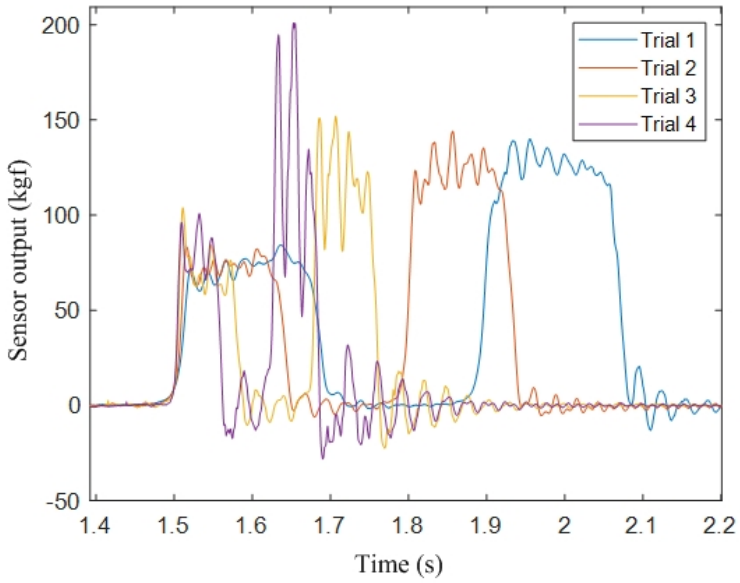

Fig. 4.7 Sensor output in "driving mode" with PCX125

Evaluation of the effect of transfer load

The theory of dynamic force balance indicates the need for considering the transfer load. However, the effect seems to be very small numerically under a constant speed. Tables 4.8, 4.9, and 4.10 present the estimation results without consideration of the transfer load. As can be seen from the tables, the estimation results look slightly worse.

Table 4.5 Estimation results with motorbike PCX125 with consideration of the transfer load

No	Velocity (km/h)	Front load (kgf)	Front error (%)	Rear load (kgf)	Rear error (%)	Gross weight (kgf)	Gross error (%)
Trial 1	10.5	73.0	-7.3	120.7	-3.5	193.7	-5.0
Trial 2	13.7	72.3	-8.2	119.1	-4.2	192.2	-5.8
Trial 3	22.6	66.6	-15.5	119.9	-4.1	186.5	-8.5
Trial 4	32.7	83.0	5.3	123.7	-1.1	206.7	1.4

Table 4.6 Estimation results with motorbike CBR1100 with consideration of the transfer load

No	Velocity (km/h)	Front load (kgf)	Front error (%)	Rear load (kgf)	Rear error (%)	Gross weight (kgf)	Gross error (%)
Trial 1	9.9	139.8	-6.5	162.3	-3.6	302.1	-5.0
Trial 2	11.8	126.5	-15.4	172.6	2.6	299.1	-5.9
Trial 3	22.8	141.4	-5.4	159.1	-5.5	300.5	-5.4
Trial 4	24.4	148.6	-0.6	155.1	-7.9	303.7	-4.4

Table 4.7 Estimation results with motorbike XR250 with consideration of the transfer load

No	Velocity (km/h)	Front load (kgf)	Front error (%)	Rear load (kgf)	Rear error (%)	Gross weight (kgf)	Gross error (%)
Trial 1	21.5	84.7	-1.4	93.1	-8.3	177.8	-5.1
Trial 2	23.6	86.2	0.4	92.9	-8.5	179.1	-4.5
Trial 3	25.8	80.9	-5.8	111.2	9.6	192.1	2.5
Trial 4	40.1	93.3	8.6	85.4	-15.9	178.7	-4.6

Table 4.8 Estimation results with motorbike PCX125 without consideration of the transfer load

No	Velocity (km/h)	Front load (kgf)	Front error (%)	Rear load (kgf)	Rear error (%)	Gross weight (kgf)	Gross error (%)
Trial 1	10.5	70.9	-10.1	122.8	-1.8	193.7	-5.0
Trial 2	13.7	71.6	-9.2	120.6	-3.6	192.2	-5.8
Trial 3	22.6	69.5	-11.7	117.0	-6.5	186.5	-8.5
Trial 4	32.7	80.5	2.2	126.2	0.8	206.7	1.4

Table 4.9 Estimation results with motorbike CBR1100 without consideration of the transfer load

No	Velocity (km/h)	Front load (kgf)	Front error (%)	Rear load (kgf)	Rear error (%)	Gross weight (kgf)	Gross error (%)
Trial 1	9.9	133.2	-10.9	168.9	0.4	302.1	-5.0
Trial 2	11.8	134.1	-10.3	165.0	-2.0	299.1	-5.9
Trial 3	22.8	132.6	-11.3	167.9	-0.2	300.5	-5.4
Trial 4	24.4	146.4	-2.1	157.3	-6.5	303.7	-4.4

Table 4.10 Estimation results with motorbike XR250 without consideration of the transfer load

No	Velocity (km/h)	Front load (kgf)	Front error (%)	Rear load (kgf)	Rear error (%)	Gross weight (kgf)	Gross error (%)
Trial 1	21.5	78.9	-8.1	98.9	-2.6	177.8	-5.1
Trial 2	23.6	69.9	-18.6	109.2	7.5	179.1	-4.5
Trial 3	25.8	89.3	4.0	102.8	1.2	192.1	2.5
Trial 4	40.1	71.8	-16.4	106.9	5.3	178.7	-4.6

Driving mode during accelerative condition

To certify the influence of acceleration and deceleration (braking) of the motorbike on the measurement device, the experiments were performed using PCX125. Figures 4.8 and 4.9 show the sensor signals under acceleration and deceleration, respectively. Each figure presents the signals obtained by three trials. According to the theory indicating the different influences in section 2.1, the graphs of the figures show the influence of acceleration and deceleration quantitatively. That is, the front axle load becomes much lower than its static load, and the rear axle load becomes higher than its static load under acceleration. The case of deceleration is a contrast to the acceleration condition. As a result, it is important to consider whether the vehicle is accelerating, decelerating, or traveling at a constant speed.

Tables 4.11 and 4.12 show the estimated results of axle loads without considering the transfer load, including acceleration and deceleration, respectively. Tables 4.13 and 4.14 show those with considering transfer load. The results show that it is compensable for static axle load estimation to consider the transfer load. Note here that using a single measurement device may cause the errors due to time detection when the wheel gets on and gets off the loading plate (as mentioned in Chapter 3). The errors of time detection lead to the errors of accelerated rates and load transfer calculations. Therefore, although the estimation of gross weight has acceptable accuracy, the axle weight for the cases of acceleration and deceleration is still limited.

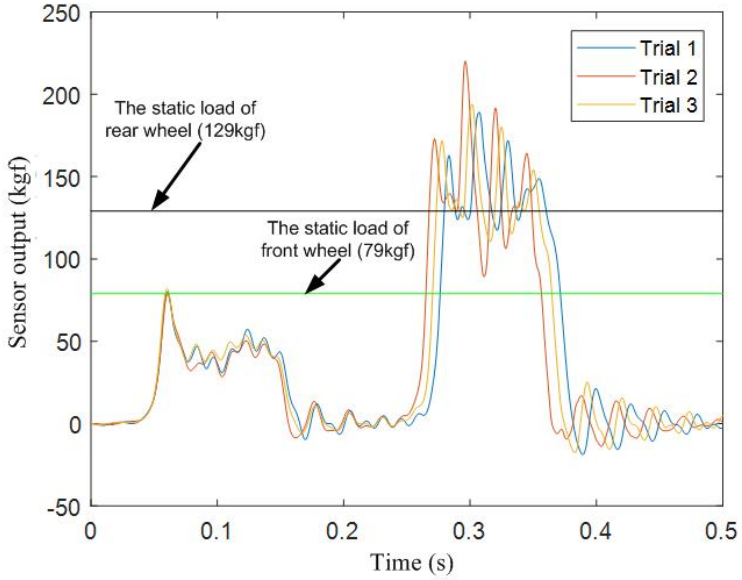

Fig. 4.8 Sensor outputs for three different trials in acceleration condition

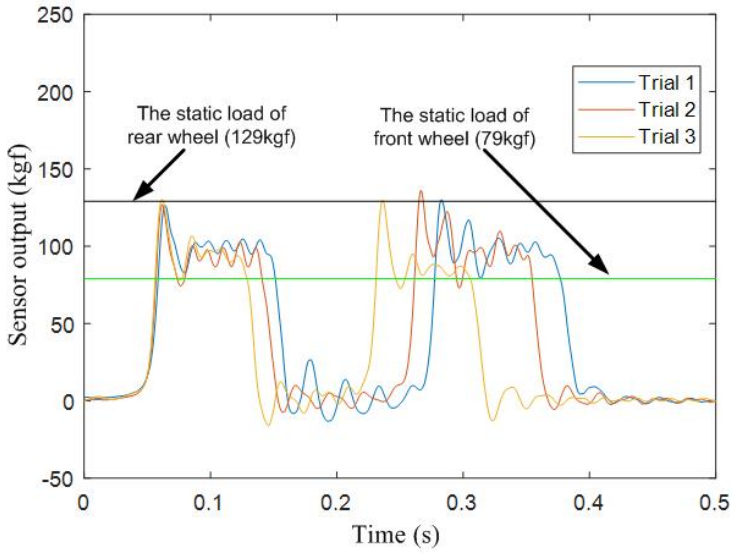

Fig. 4.9 Sensor outputs for three different trials in deceleration condition

Table 4.11 Estimation results in acceleration condition without consideration of the transfer load

No	Velocity (km/h)	Acc. (m/s^2)	Front load (kgf)	Front error (%)	Rear load (kgf)	Rear error (%)	Gross weight (kgf)	Gross error (%)
Trial 1	17.5	0.7	44.8	-43.3	136.5	9.1	181.3	-11.1
Trial 2	17.7	0.3	46.4	-41.3	134.9	7.9	181.3	-11.1
Trial 3	18.9	1.3	43.2	-45.4	142.4	13.8	185.5	-9.0

Note: Acc: the rate of acceleration

Table 4.12 Estimation results in deceleration condition without consideration of the transfer load

No	Velocity (km/h)	Acc. (m/s^2)	Front load (kgf)	Front error (%)	Rear load (kgf)	Rear error (%)	Gross weight (kgf)	Gross error (%)
Trial 1	17.7	-1.7	98.9	25.5	97.5	-22.1	196.4	-3.7
Trial 2	18.6	-2.3	92.8	17.7	97.7	-21.9	190.5	-6.6
Trial 3	21.8	-1.0	94.6	20.1	86.4	-30.9	181.0	-11.2

Table 4.13 Estimation results in acceleration condition with consideration of the transfer load

No	Velocity (km/h)	Acc. (m/s^2)	Front load (kgf)	Front error (%)	Rear load (kgf)	Rear error (%)	Gross weight (kgf)	Gross error (%)
Trial 1	17.5	0.7	49.5	-37.1	131.8	5.3	181.3	-11.1
Trial 2	17.7	0.3	48.5	-38.4	132.8	6.2	181.3	-11.1
Trial 3	18.9	1.3	51.8	-34.3	133.8	6.9	185.5	-9.0

Table 4.14 Estimation results in deceleration condition with consideration of the transfer load

No	Velocity (km/h)	Acc. (m/s^2)	Front load (kgf)	Front error (%)	Rear load (kgf)	Rear error (%)	Gross weight (kgf)	Gross error (%)
Trial 1	17.7	-1.7	87.0	10.4	109.4	-12.6	196.4	-3.7
Trial 2	18.6	-2.3	76.6	-2.8	113.9	-8.9	190.5	-6.6
Trial 3	21.8	-1.0	88.0	11.7	93.0	-25.6	181.0	-11.2

Estimation results with a consideration of underestimation

As mentioned at the beginning of this section, the estimation results above are calculated based on the algorithm presented in Section 2.2.2. Here, we consider about the results with consideration of underestimation as presented in Section 2.2.3. Table 4.15 shows the results obtained from two algorithms.

Table 4.15 Comparison of two averaging methods

No	Velocity (km/h)	Front load (kgf)	N-Front load (kgf)	Rear load (kgf)	N-Rear load (kgf)	Gross weight (kgf)	Gross error (%)	N-Gross weight (kgf)	N-Gross error (%)
Trial 1	10.5	70.9	71.5	122.8	123.2	193.7	-5.0	194.7	-4.5
Trial 2	13.7	71.6	71.7	120.6	121.2	192.2	-5.8	192.9	-5.4
Trial 3	18.1	65.0	64.7	126.2	126.4	191.3	-6.2	191.1	-6.3
Trial 4	26.5	82.9	81.3	105.3	102.7	188.3	-7.7	184.0	-9.8
Trial 5	31.5	72.6	75.0	134.0	128.6	206.6	1.3	203.6	-0.2
Trial 6	32.7	80.5	80.1	126.2	125.4	206.7	1.4	205.4	0.7

Note: N-Front, N-Rear and N-Gross are front load, rear load and gross weight, respectively. The results of estimation by applying the algorithm in Section 2.2.3.

Note that, we do not consider transfer load in these cases. So, the estimation of axle load and gross weight without transfer loads are investigated. Regarding the table, the results of the new algorithm in Section 2.2.3 are slightly smaller than the one in section 2.2.2 and underestimation. The later sections have presented the results of estimation by applying the algorithm in Section 2.2.3.

4.2 Experiments with two measurement devices

The experiments are conducted with a motorbike PCX 125 at a place in Tokyo Institute of Technology's campus. Table 4.16 shows the static axle loads of the test motorbike including the weight of a driver. The weights are measured in the stationary condition using a digital platform scale on the site prior to the experiment of WIM. It is verified that the static axle loads vary about ±4 kgf from the values in Table 4.16. The fluctuation of ±4 kgf is observed by depending on changing the rider's body posture forward and backward on the seat.

Table 4.16 The weight of the motorbike including driver by stationary weighing

Model of motorbike	Front (kgf)	Rear load (kgf)	Gross weight (kgf)
PCX125	78	131	209

Note: the measurement varies about ±4 kgf depending on changing the rider's body posture forward and backward on the seat.

4.2.1 Experiment with constant speed

Figure 4.10 shows the sensor signal data of four experimental runs in constant speed conditions. Note here that the test rider tried to drive the motorbike at constant speeds but the small fluctuation of speed might be unavoidable. Since a test motorbike runs on two measurement devices with a distance of 2.3 meters, the signal data of each trial has four rectangular risings in signal in time domain with some degrees of vibration. The time distances between the rising points due to the axle load of the front and the rear wheel differ according to the different speed of the motorbike. The time distances between the rising points in signals from the first device and the second one also differs. Table 4.17 shows the estimation results from the data. It is unnecessary to consider transfer load in this estimation because of almost constant speeds. The axle loads are obtained through the averaging two estimations by the first and the second measurement device. As can be seen in the table, the estimation errors are small. The gross errors are smaller than 3% (4/4 trials).

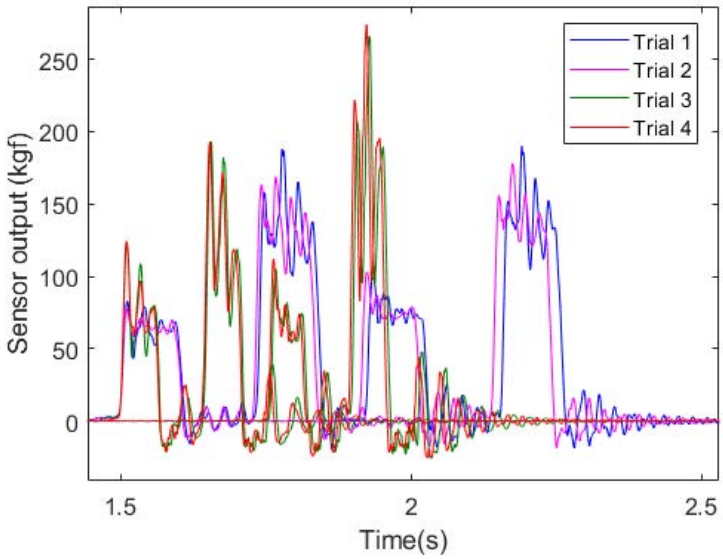

Fig. 4.10 Sensor outputs in constant speeds

Table 4.17 The estimation results in constant speed condition

No	Velocity (km/h)	Front load (kgf)	Front error (%)	Rear load (kgf)	Rear error (%)	Gross weight (kgf)	Gross error (%)
Trial 1	19.9	71.2	-8.7	135.5	3.5	206.8	-1.1
Trial 2	20.3	71.9	-7.8	133.9	2.2	205.7	-1.6
Trial 3	32.9	79.2	1.6	132.7	1.3	211.9	1.4
Trial 4	33.2	77.3	-0.9	138.0	5.3	215.2	3.0

Note: Errors in three columns are calculated using the values in Table 4.16 for Ws by Eq. 4.1.

4.2.2 Experiment during accelerative condition

Figure 4.11 and 4.12 show the sensor signal data of experiments in the cases of accelerated movement and deceleration. As can be seen in the figures, the influence of acceleration and deceleration is noticeable. In accelerated condition, the front axle load becomes much lower than its static load, and the rear axle load becomes higher. The case of deceleration contrasts with the accelerated condition.

Tables 4.18 and 4.19 show the estimation results from the data. In table 4.18, the estimation errors are shown in round brackets. The errors of the front and rear wheels with consideration of transfer load are much smaller than without the consideration. Also, the errors of both wheels are bigger than of the gross weight. However, the static front and rear axle loads fluctuate in the range of 74–82 kgf and 127–135 kgf, respectively, depending on the position of the seated rider's upper body in the static measurement in this study. Therefore, the estimation results are still considered acceptably accurate. Note here that the information about the height of the mass center of vehicles is required and that the acceleration rate should be almost constant while the vehicles run over the two measurement devices.

Table 4.18 Estimation results in acceleration condition

No	Velocity (km/h)	Acc. (m/s^2)	Front load (kgf) (without TF)	Rear load (kgf) (without TF)	Gross weight (kgf) (without TF)	Front load (kgf) (with TF)	Rear load (kgf) (with TF)	Gross weight (kgf) (with TF)
Trial 1	25.7	1.5	54.1 (-30.6%)	150.6 (14.9%)	204.6 (-2.1%)	71.6 (-8.2%)	133.1 (1.6%)	204.6 (-2.1%)
Trial 2	26.8	1.7	51.7 (-33.8%)	150.5 (14.9%)	202.2 (-3.3%)	71.3 (-8.6%)	130.9 (-0.1%)	202.2 (-3.3%)
Trial 3	27.0	1.5	56.9 (-27.0%)	151.0 (15.3%)	207.9 (-0.5%)	75.2 (-3.6%)	132.7 (1.3%)	207.9 (-0.5%)

Note: Acc: the rate of acceleration without TF and with TF: without and with consideration of transfer load errors in round brackets: calculation by Eq. 4.1 referring the static axle loads in Table 4.16

Table 4.19 Estimation results in deceleration condition

No	Velocity (km/h)	Acc. (m/s^2)	Front load (kgf) (without TF)	Rear load (kgf) (without TF)	Gross weight (kgf) (without TF)	Front load (kgf) (with TF)	Rear load (kgf) (with TF)	Gross weight (kgf) (with TF)
Trial 1	23.7	-1.7	94.9 (21.7%)	105.6 (-19.4%)	200.6 (-4.0%)	76.0 (-2.6%)	124.6 (-4.9%)	200.6 (-4.0%)
Trial 2	25.2	-1.6	101.3 (29.9%)	101.3 (-22.6%)	202.7 (-3.0%)	82.8 (6.1%)	119.9 (-8.5%)	202.7 (-3.0%)
Trial 3	26.2	-2.2	107.8 (38.2%)	94.8 (-27.6%)	202.6 (-3.1%)	82.5 (5.8%)	120.1 (-8.4%)	202.6 (-3.1%)
Trial 4	27.0	-2.0	103.7 (33.0%)	98.1 (-25.1%)	201.8 (-3.4%)	80.9 (3.7%)	120.9 (-7.7%)	201.8 (-3.4%)

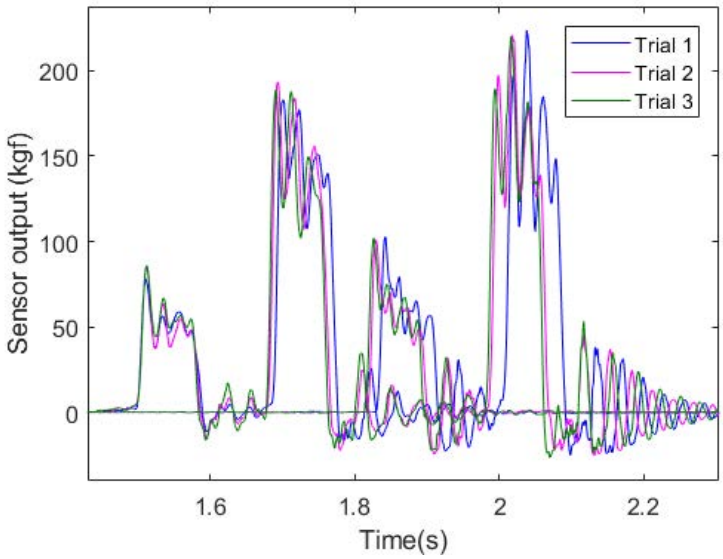

Fig. 4.11 Sensor outputs for three trials in acceleration condition

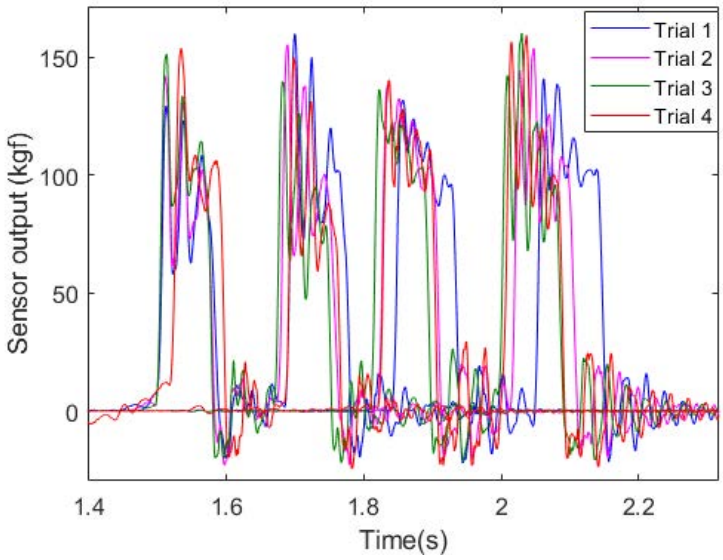

Fig. 4.12 Sensor outputs for four trials in deceleration condition

4.3 Experiments with a single measurement device for a light truck

Experiments were conducted with a light truck Sambar on the campus of Tokyo Tech University. As discussed in Section 2.4, the experiment is conducted with two sides of the truck: left (Fig. 4.13) and right directions (Fig. 4.14). Table 4.20 shows the static weights of each side, including the weight of a driver, measured on the site prior before conducting experiments. Experiments were conducted with constant speed, accelerated motion (acceleration and deceleration conditions).

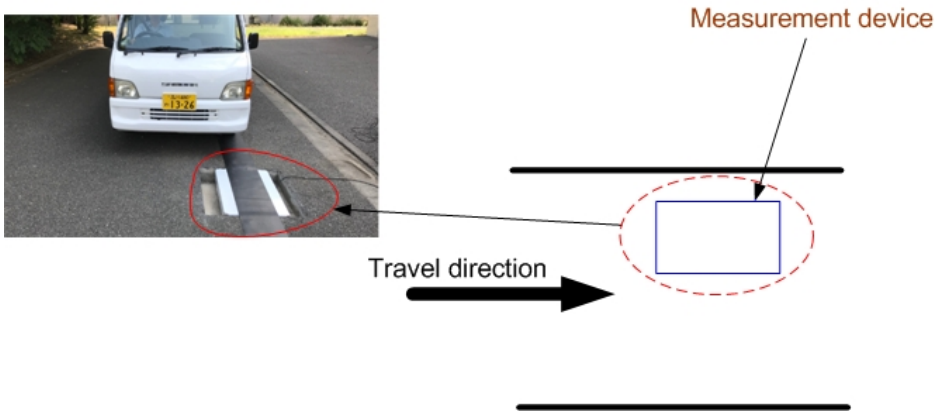

Fig. 4.13 Experiments with left side of the truck

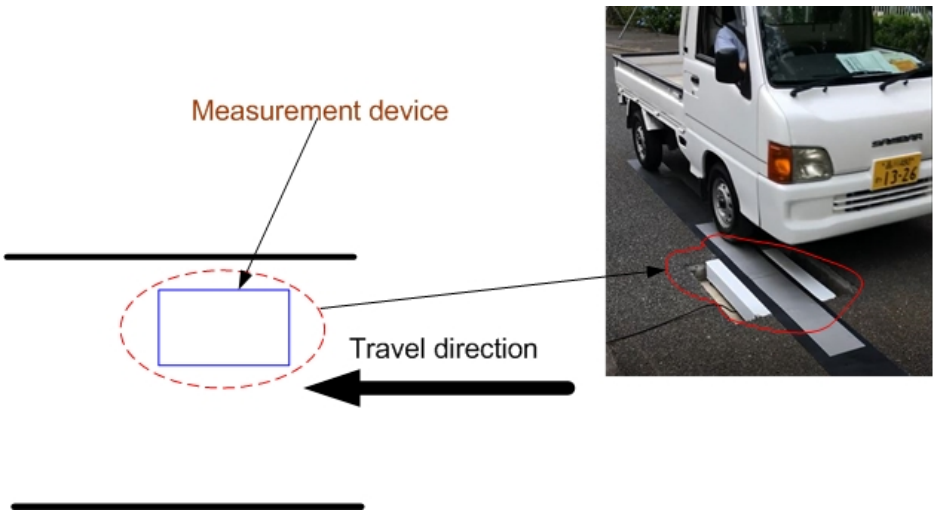

Fig. 4.14 Experiments with right side of the truck

Table 4.20 The weight of the truck including the rider measured on the site of experiments

Sides	Front load (kgf)	Rear load (kgf)	Half-car load (kgf)
Left	235.0	178.0	413.0
Right	264.0	206.0	470.0

Note: including the weight of rider on seat

4.3.1 Driving mode with constant speed

The true static weights of the light truck for both sides (Table 4.20) with a driver are measured before the experiments. Figures 4.15 and 4.16 show the sensor signal data of experiments of both sides. Tables 4.21 and 4.22 show the estimated wheel loads and half-car load from the signal data of the left and right sides, respectively. As can be seen from the tables, the estimation results with constant speeds have high accuracy. The estimation errors of half-car load are less than 3% (with 15/16 trials). The estimation errors of wheel loads (front and rear wheels of both sides) are smaller than 5% (29/32 cases). Therefore, according to COST 323 [10], this system can be considered as class A(5) for both half-car load and axle load.

Compared to the estimation results for motorcycles in the previous section, we can see that the estimation results for the truck have much higher accuracy. There are several reasons for these measurement results. Firstly, because the measurement device for a light truck is installed with the same level as the road, the output signals are less influence by shock vibration and vertical oscillation of the vehicle. Secondly, because of the size of equipment for trucks larger than the one for motorcycles, the time signal history is much better to apply the averaging method. Thirdly, trucks are less affected by roll motion than motorbikes.

Table 4.21 The estimation results in constant speed condition (left side)

No	Velocity (km/h)	Front load (kgf)	Front error (%)	Rear load (kgf)	Rear error (%)	Half-car load (kgf)	Half-car error (%)
Trial 1	8.5	238.1	1.3	182.8	2.7	420.9	1.9
Trial 2	22.4	233.5	-0.6	183.9	3.3	417.4	1.1
Trial 3	22.7	225.4	-4.1	188.5	5.9	413.9	0.2
Trial 4	24.7	225.8	-3.9	185.5	4.2	411.3	-0.4
Trial 5	25.5	226.5	-3.6	182.0	2.2	408.5	-1.1
Trial 6	26.5	222.3	-5.4	172.2	-3.3	394.5	-4.5
Trial 7	26.8	225.9	-3.9	186.8	4.9	412.7	-0.1
Trial 8	27.5	234.2	-0.4	179.8	1.0	414.0	0.2

Note: Errors in three columns are calculated using the values in Table 4.20 for W_s by Eq. (4.1).

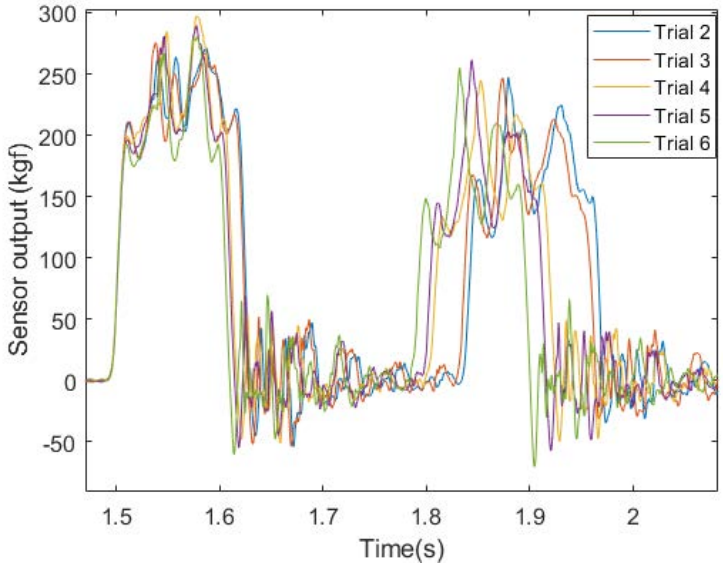

Fig. 4.15 Sensor outputs in constant speeds (left side)

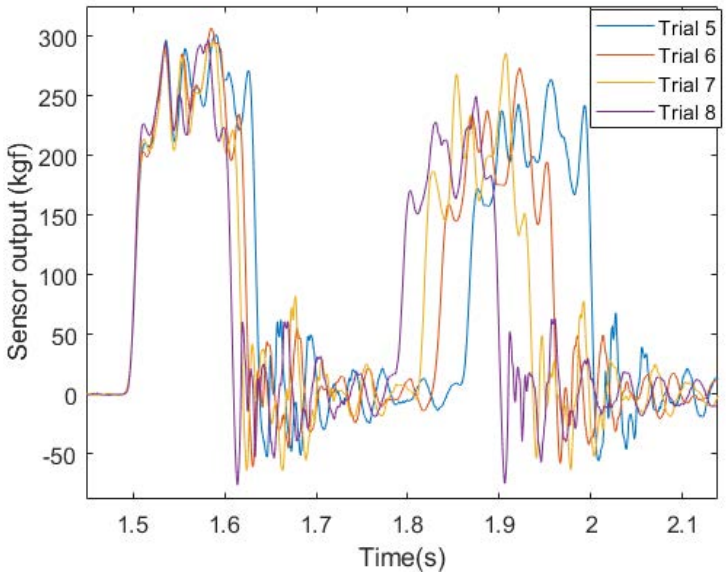

Fig. 4.16 Sensor outputs in constant speeds (right side)

Table 4.22 The estimation results in constant speed condition (right side)

No	Velocity (km/h)	Front load (kgf)	Front error (%)	Rear load (kgf)	Rear error (%)	Half-car load (kgf)	Half-car error (%)
Trial 1	8.1	264.5	0.2	207.3	0.6	471.7	0.4
Trial 2	8.4	267.5	1.3	207.3	0.6	474.8	1.0
Trial 3	8.5	269.2	2.0	209.3	1.6	478.5	1.8
Trial 4	8.7	267.0	1.1	209.7	1.8	476.7	1.4
Trial 5	20.5	258.0	-2.3	205.7	-0.1	463.7	-1.3
Trial 6	22.4	252.7	-4.3	207.7	0.8	460.3	-2.1
Trial 7	24.1	248.9	-5.7	213.5	3.6	462.4	-1.6
Trial 8	26.2	251.8	-4.6	204.2	-0.9	456.0	-3.0

4.3.2 Driving mode with acceleration condition

Figures 4.17 and 4.18 show the sensor signal data of experiments of both sides. Tables 4.23 and 4.24 show the estimated wheel loads and half-car load from the signal data of the left and right sides, respectively. The estimation errors are shown in round brackets.

According to the figures, the load transferring from the front and rear wheels. The estimation results are acceptable accuracy. The errors of the front and rear wheels with consideration of transfer load are much smaller than without the consideration. The estimation errors of the half-car load are less than 8% (6/6 trials). The estimation errors of wheel loads are less than 8% (11/12 cases). The estimation results of the rear wheel are much better than the front wheel. Compared to the estimation results for motorcycles in the previous sections, we can see that the estimation results for the truck have much higher accuracy. According to COST 323 [10], the system can be considered as B(10) class.

Table 4.23 Estimation results in acceleration condition (left side)

No	Velocity (km/h)	Acc. (m/s^2)	Front load (kgf) (without TF)	Rear load (kgf) (without TF)	Half-car load (kgf) (without TF)	Front load (kgf) (with TF)	Rear load (kgf) (with TF)	Half-car loadd (kgf) (with TF)
Trial 1	23.6	0.4	212.1 (-9.7 %)	176.5 (-0.8 %)	388.6 (-5.9 %)	217.0 (-7.7 %)	171.7 (-3.6 %)	388.6 (-5.9 %)
Trial 2	25.4	1.3	202.3 (-13.9 %)	187.6 (5.4 %)	389.8 (-5.6 %)	219.5 (-6.6 %)	170.3 (-4.3 %)	389.8 (-5.6 %)
Trial 3	25.5	1.0	200.0 (-14.9 %)	183.4 (3.0 %)	383.4 (-7.2 %)	213.0 (-9.3 %)	170.4 (-4.3 %)	383.4 (-7.2 %)

Note: Acc: the rate of acceleration without TF and with TF: without and with consideration of transfer load errors (%): calculation by Eq. (4.1) referring the static axle loads in Table 4.20

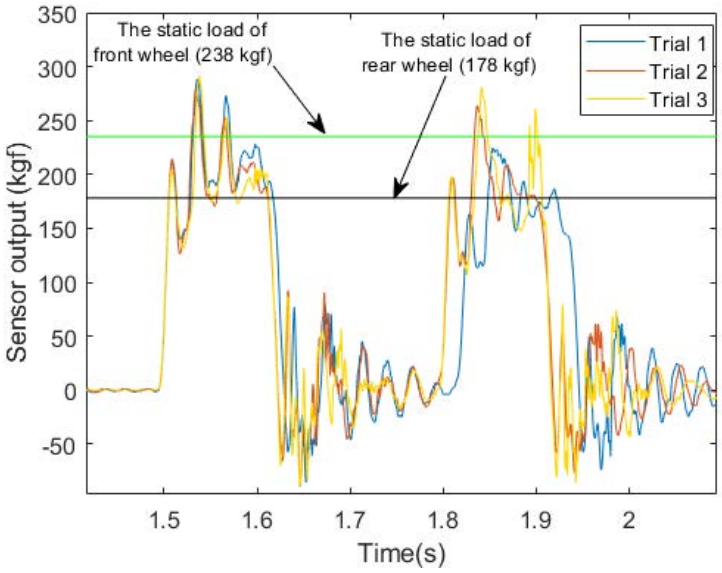

Fig. 4.17 Sensor outputs in acceleration condition (left side)

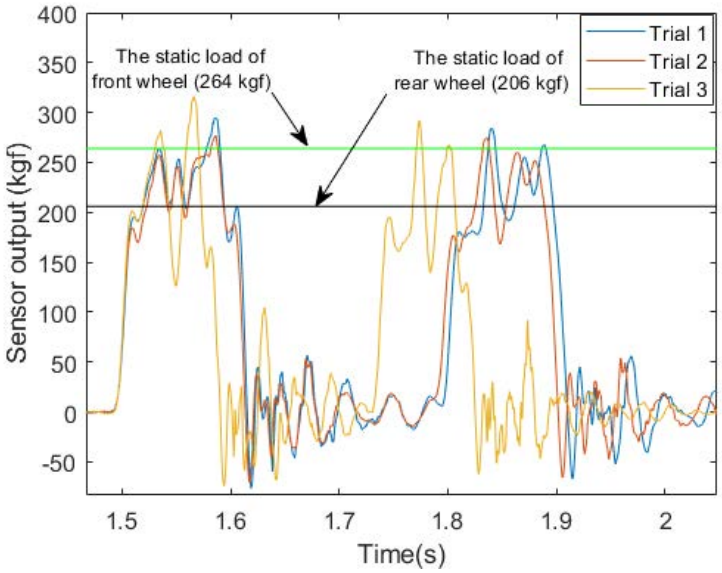

Fig. 4.18 Sensor outputs in acceleration condition (right side)

Table 4.24 Estimation results in acceleration condition (right side)

No	Velocity (km/h)	Acc. (m/s^2)	Front load (kgf) (without TF)	Rear load (kgf) (without TF)	Half-car load (kgf) (without TF)	Front load (kgf) (with TF)	Rear load (kgf) (with TF)	Half-car load (kgf) (with TF)
Trial 1	25.8	0.9	234.9 (-11.0 %)	223.9 (8.70 %)	458.8 (-2.4 %)	249.1 (-5.7 %)	209.7 (1.8 %)	458.8 (-2.4 %)
Trial 2	26.3	1.8	228.8 (-13.3 %)	223.0 (8.30 %)	451.8 (-3.9 %)	256.1 (-3.0 %)	195.7 (-5.0 %)	451.8 (-3.9 %)
Trial 3	32.9	0.9	230.4 (-12.7 %)	209.1 (1.50 %)	439.4 (-6.5 %)	244.5 (-7.4 %)	194.9 (-5.4 %)	439.4 (-6.5 %)

4.3.3 Driving mode with deceleration condition

Figures 4.19 and 4.20 show the sensor signal data of experiments of both sides in deceleration condition. Tables 4.25 and 4.26 show the estimated wheel loads and half-car load from the signal data of the left and right sides, respectively. Contrast to the acceleration condition, the load transferring from the rear to front wheels in the deceleration condition. The estimation results are acceptable accuracy. The estimation errors of the half-car load are less than 8% (7/7 trials). The estimation errors of wheel loads are less than 10% (12/14 cases). The estimation results of the rear wheel are much better than the front wheel. Similar to the acceleration condition, we can see that the estimation results for the truck have much higher accuracy compared to the estimation results for motorcycles in the previous section. According to COST 323 [10], the system can be considered as B(10) class.

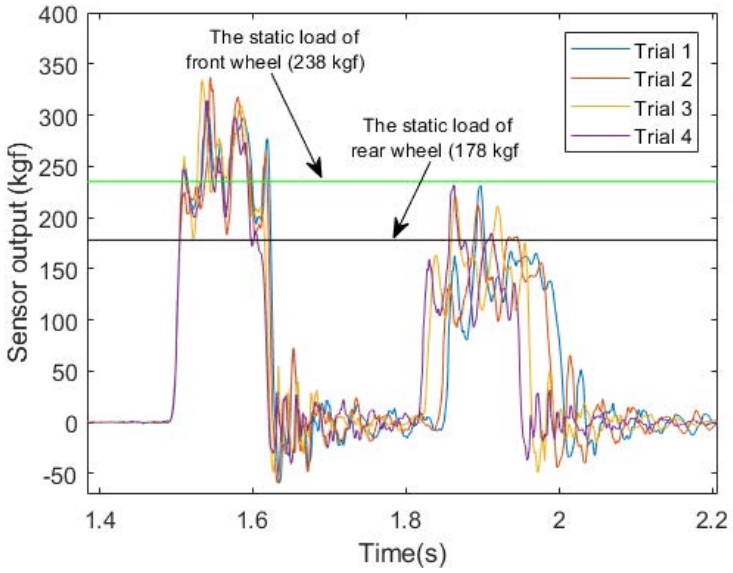

Fig. 4.19 Sensor outputs in deceleration condition (left side)

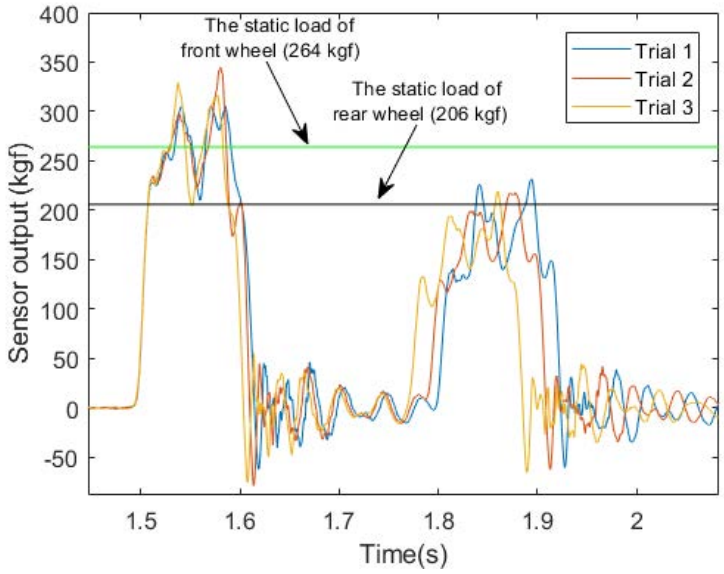

Fig. 4.20 Sensor outputs in deceleration condition (right side)

Table 4.25 Estimation results in deceleration condition (left side)

No	Velocity (km/h)	Acc. (m/s^2)	Front load (kgf) (without TF)	Rear load (kgf) (without TF)	Half-car load (kgf) (without TF)	Front load (kgf) (with TF)	Rear load (kgf) (with TF)	Half-car load (kgf) (with TF)
Trial 1	19.8	-2.8	252.1 (7.3%)	147.2 (-17.3 %)	399.3 (-3.3 %)	216.1 (-8.1 %)	183.2 (2.9%)	399.3 (-3.3 %)
Trial 2	20.4	-2.3	243.1 (3.4%)	148.6 (-16.5 %)	391.7 (-5.2 %)	213.3 (-9.2 %)	178.3 (0.2%)	391.7 (-5.2 %)
Trial 3	21.5	-2.4	252.2 (7.3%)	156.4 (-12.2 %)	408.6 (-1.1 %)	220.6 (-6.1 %)	188.0 (5.6%)	408.6 (-1.1 %)
Trial 4	21.9	-1.7	237.6 (1.1%)	149.5 (-16.0 %)	387.2 (-6.3 %)	216.9 (-7.7 %)	170.2 (-4.4 %)	387.2 (-6.3 %)

Note: Acc: the rate of acceleration without TF and with TF: without and with consideration of transfer load errors (%): calculation by Eq. (4.1) referring the static axle loads in Table 4.20

Table 4.26 Estimation results in deceleration condition (right side)

No	Velocity (km/h)	Acc. (m/s^2)	Front load (kgf) (without TF)	Rear load (kgf) (without TF)	Half-car load (kgf) (without TF)	Front load (kgf) (with TF)	Rear load (kgf) (with TF)	Half-car load (kgf) (with TF)
Trial 1	25.6	-1.4	266.0 (0.8%)	175.0 (-15.0 %)	441.0 (-6.2 %)	245.8 (-6.9 %)	195.2 (-5.2 %)	441.0 (-6.2 %)
Trial 2	26.5	-2.0	264.1 (0.1%)	174.8 (-15.2 %)	438.9 (-6.6 %)	236.4 (-10.4 %)	202.5 (-1.7 %)	438.9 (-6.6 %)
Trial 3	28.0	-2.8	267.8 (1.4%)	167.2 (-18.8 %)	435.0 (-7.4 %)	229.2 (-13.2 %)	205.8 (-0.1 %)	435.0 (-7.4 %)

4.4 Summary

In this chapter, experiments with motorcycles and light trucks carried out to verify estimation algorithms are presented in Chapter 3. The results of experiments using only one miniature measurement device and motorbikes were obtained mostly with acceptable accuracy in the cases of “walking mode” and “driving mode” under constant speed conditions. Most estimations of gross weight were reliably accurate, with errors smaller than 6%. Most results were obtained as slightly underestimated values.

The results of an experimental study using two measurement devices and a motorbike were presented to demonstrate the improvement of the estimation algorithm, as shown in Section 2.3. It was found that averaging the axle loads obtained using two measurement devices has the potential to enhance the reliability and the accuracy of axle load estimation. The errors of the estimation of gross weight in accelerated conditions are less than 5%, which were more accurate than the results of the experiments using a single measurement device.

Compared to the estimation results of motorbikes using a single measurement device, the estimation results for a light truck were better not only half-car loads but also axle loads (each side). The errors of half-car loads (each side) were under 3%, while errors of wheel load were under 5% in cases of constant speed. In cases of acceleration or deceleration, the estimation errors were under 8%. The system can be considered as A(5) class in the constant speed and B(10) in acceleration and deceleration conditions. Note that the road surface used in the experiment is not standard like the roads for commercial WIM. Also, road construction and installation for measurement device are still simple. However, the estimation results are highly accurate.

Chapter 5

Conclusions and future work

5.1 Conclusions

Weigh-in-Motion, WIM, in brief, is the technology for estimating static axle load of vehicles in motion. It has been developed to detect overload trucks, which may cause the damage of traffic infra-structures, a high risk of traffic accidents, and the unfair of freight transportation.

The most important part of the WIM system is the static load estimation algorithm for the vehicles in motion. There are studies on estimation methods of both BWIM and pavement WIM. However, they are still having limitations such as time-consuming calibration, high errors, or computation load. More importantly, those studies are based on the assumption that vehicles run at a constant speed. In actual operation, the vehicles do not always run at constant speeds. In cases of accelerative motion, the axle weights are significantly influenced by the transfer load from front to rear wheels and vice versa.

This research proposed a new axle load estimation algorithm of a vehicle in motion based on an averaging method using plate-type measurement devices. The algorithm can estimate the static load with slight underestimate.It is available for vehicle in motion not only with constant but also non-constant speeds.The estimation algorithm using two measurement device placed in cascade layout is also proposed. In this research, three miniature measurements devices (plate-type) were developed and used for conducting experiments using motorbikes and a light truck. The validity and accuracy of the proposed method were investigated by means of experimental ways using motorbikes and a light truck. Experimental results showed that the WIM system in this research can estimate the axle loads of test vehicles with practically acceptable accuracy using a single device. It is also found that the reliability and accuracy of axle load estimation are increased compared to the usage of a single device. The result of this WIM system in this research can estimate the axle loads of test vehicles with

acceptable accuracy in B(10) class, according to COST323. This research can stimulate the development of practical future Weigh-in-Motion of heavy-duty trucks.

5.2 Future works

Based on the initial results of this research, future works will focus on the development of the full WIM system.

5.2.1 Hardware

Improvement of measurement device

The measurement devices need to be developed with suitable size, insensitive with the vertical force position, high damping, high signal-noise-ratio and with high capacity for a load of a heavy truck's axles. The current system is still has some limitations of load capacity. In the near feature, the research needs to improve the measurement device to conduct experiment with heavier trucks.

Automatic classification system

In the WIM system, the vehicle classification system also plays an important role, especially for the cases of accelerative motion. Therefore, it is crucial to develop the classification system based on the parameters obtained from the results of static load estimation and the recognition system based on image processing.

5.2.2 Software

Improving the estimation algorithm

The errors of estimation results using one measurement device in the cases of accelerative motion are still higher than the ones of constant speeds. These errors are higher not only axle weights but also gross weight. The influences of accelerative motion may be caused by the effects of friction or vibration factors. The current estimation method did not consider these factors. In the near future, the research needs to consider these factors to increase the estimation results.

Real-time software

The author will complete the real-time software connecting all hardware system. The software needs to be developed with the graphical user interface (GUI).

5.2.3 Experiments

Conducting experiments with both sides of truck

In the near future, the experiments with both sides of a light truck will be conducted.

Bibliography

[1] Ghosn M., Fiorillo G., Gayovyy V., Getso T., Ahmed S., and Parker N. Effects of overweight vehicles on NYSDOT infrastructure. Tech Report C-08-13, University Transportation Research Center, 2015.

[2] Sandy H. Straus and John Semmens. Estimating the cost of overweight vehicle travel on Arizona highways. Tech Report FHWA-AZ-06-528, Arizona Department of Transportation, 2006.

[3] Sinha K., Labi S., Rodriguez M., Tine G., and Dutta R. Procedures for the estimation of pavement and bridge preservation costs for fiscal planning and programming. Tech Report FHWA/IN/JTRP-2005/17, Indiana Department of Transportation, 2005.

[4] Harwood W., Torbic J., Richard R., Ghanz D., and Eleferiadou L. Review of truck characteristics as factors in roadway design. NCHRP report 505, Transportation Research Board, 2003.

[5] Hans van Loo and Ales Znidaric. *Guide for Users of Weigh-In-Motion*. ISWIM, Czech, 2019.

[6] Hidehiko Sekiya, Kentaro Kimura, and Chitoshi Miki. Technique for determining bridge displacement response using mems accelerometers. *Sensors*, 16(2), 2016.

[7] C. Koniditsiotis and B. Peters. Weigh-in-motion technology. *National Library of Australia*, 2000.

[8] Marek Bistak, František Brumerčík, and Michal Lukáč. Weighing systems in traffic. *Zeszyty Naukowe. Transport/Politechnika Śląska*, 2017.

[9] Burnos Piotr and Gajda Janusz. Vehicle's Weigh-in-motion system for enforcement in Poland. In *Proceedings of 11th ITS European Congress, Glasgow*, 05/ 2016.

[10] Jacob B., E. O'Brien, and S. Jehaes. Weight-in-motion of road vehicles: final report of the COST 323 action (WIM-LOAD) COST 323 (1993 - 1998). ISBN: 2-7202-3096-8, 2002.

[11] ASTM E-1318. Standard specifications for highway weigh-in-motion (WIM) systems with user requirements and test methods. ISBN: 2-7202-3096-8, 2009.

[12] Yu Yang, Cai C., and Deng Lu. State-of-the-art review on bridge weigh-in-motion technology. *Advances in Structural Engineering*, 19, 06 2016.

[13] Eugene J. O'Brien, Ales Znidaric, Werner Baumgärtner, Arturo González, and Peter McNulty. Weighing-in-motion of axles and vehicles for europe (WAVE) WP1.2: Bridge WIM systems, 2001.

[14] Myra Lydon, Su Taylor, D Robinson, Aftab Mufti, and Eugene OBrien. Recent developments in bridge weigh in motion (B-WIM). *Journal of Civil Structural Health Monitoring*, 6, 05 2015.

[15] Michael Quilligan, Raid Karoumi, and Eugene OBrien. Development and testing of a 2-dimensional multi-vehicle bridge-WIM algorithm. In *Proceedings of 3rd International Conference on Weigh-in-Motion, Orlando, USA*, 05 2002.

[16] W. Rowley, Eugene OBrien, Arturo Gonzalez, and Ales Znidaric. Experimental testing of a moving force identification bridge weigh-in-motion algorithm. *Experimental Mechanics*, 49:743–746, 10 2008.

[17] Eugene J. OBrien, Cillian W. Rowley, Arturo Gonzalez, and Mark F. Green. A regularised solution to the bridge weigh-in-motion equations. *International Journal of Heavy Vehicle Systems*, 16(3):310–327, 2009.

[18] Raid Karoumi, Michael Quilligan, and Eugene OBrien. Calculating an influence line from direct measurements. *Proceedings of The Ice - Bridge Engineering*, 159:31–34, 01 2006.

[19] Gunnstein T. Frøseth, Anders Rønnquist, Daniel Cantero, and Ole Øiseth. Influence line extraction by deconvolution in the frequency domain. *Computers & Structures*, 189:21 – 30, 2017.

[20] T.H.T. Chan, S.S. Law, T.H. Yung, and X.R. Yuan. An interpretive method for moving force identification. *Journal of Sound and Vibration*, 219(3):503 – 524, 1999.

[21] S.S. Law, T.H.T. Chan, and Q.H. Zeng. Moving force identification: A time domain method. *Journal of Sound and Vibration*, 201(1):1 – 22, 1997.

[22] S. S. Law, J. Q. Bu, X. Q. Zhu, and S. L. Chan. Vehicle condition surveillance on continuous bridges based on response sensitivity. *Journal of Engineering Mechanics*, 132(1):78–86, 2006.

[23] Pranesh Chatterjee, Eugene OBrien, Yingyan Li, and Arturo González. Wavelet domain analysis for identification of vehicle axles from bridge measurements. *Computers and Structures*, 84(28):1792 – 1801, 2006.

[24] S. S. Law, S. Q. Wu, and Z. Y. Shi. Moving load and prestress identification using wavelet-based method. *Journal of Applied Mechanics*, 75(2):021014–021014–7, 2008.

[25] Bernhard Lechner, M. Lieschnegg, O. Mariani, Martin Pircher, and A. Fuchs. A wavelet-based bridge weigh-in-motion system. *International Journal on Smart Sensing and Intelligent Systems*, 3, 12 2010.

[26] K. Liu, S.S. Law, X.Q. Zhu, and Y. Xia. Explicit form of an implicit method for inverse force identification. *Journal of Sound and Vibration*, 333(3):730 – 744, 2014.

[27] L. Deng and C.S. Cai. Identification of parameters of vehicles moving on bridges. *Engineering Structures*, 31(10):2474 – 2485, 2009.

[28] L. Deng and C.S. Cai. Identification of dynamic vehicular axle loads: Demonstration by a field study. *Journal of Vibration and Control*, 17(2):183–195, 2011.

[29] Kwon Taek. Signal processing of piezoelectric weight-in-motion systems. In *Proceedings of the 5th IASTED International Conference on Circuits, Signals and Systems*, pages 233–238, 07 2007.

[30] Umit Sonmez, Donald A. Streit, Robin Tallon, and David Klinikowski. Weigh-in-motion studies using strip-type sensors: the preliminary results. *International Journal of Heavy Vehicle Systems*, 15, 04 2008.

[31] Junichi Morikawa, Tsurumaki Atsushi, and Kato Munehiko. Overloaded vehicles and automatic axle weighing system for rapid transit installed in the Hanshin expressway. In *Proceedings of 7th International Conference on Weigh-In-Motion (ICWIM-07), Brazil*, 2016.

[32] Ahmad Saifizul Abdullah. *Development of Integrated Weigh-in-motion System and Analysis of Traffic Flow Characteristics considering Vehicle Weight*. PhD thesis, University of Tokushima, 2011.

[33] Beatrix Ronay-Tobel, Robert Mikulas, Attila Katkics, and Miklos Toldi. Weight enforcement network of Hungary (a multilevel case study on WIM). In *Proceedings of 8th International Conference on Weigh-In-Motion (ICWIM-08), Prague, Czech*, 2019.

[34] Torbjørn Haugen, Jorunn Riddervold Levy, Bjoern Branendshoei, and Maximilian Franz Böhm. Innovative use of piezoelectric speed enforcement systems for weight data collection. In *Proceedings of 8th International Conference on Weigh-In-Motion (ICWIM-08), Prague, Czech*, 2019.

[35] Cebon David and C B. Winkler. Multiple-sensor weigh-in-motion: Theory and experiments. *Transportation Research Record, TRB*, 1311, 01 1991.

[36] Delphine Labry, Victor Dolcemascolo, and Bernard Jacob. MS-WIM systems optimisation method. In *Proceedings of the 8th International Symposium on Heavy Vehicles Weights and Dimensions*, 2004.

[37] L K Stergioulas, D Cebon, and M D Macleod. Static weight estimation and system design for multiple-sensor weigh-in-motion. *Proceedings of the Institution of Mechanical Engineers, Part C: Journal of Mechanical Engineering Science*, 214(8):1019–1035, 2000.

[38] Gajda Janusz, Sroka Ryszard, Stencel Marek, Zeglen Tadeusz, Piotr Piwowar, Piotr Burnos, and Zbigniew Marszalek. Design and accuracy assessment of the multi-sensor weigh-in-motion system. In *Proceedings of IEEE International Instrumentation and Measurement Technology Conference (I2MTC)*, 05 2015.

[39] Ministère des Transports du Québec. Vehicle load and size limits guide. http://www.bv.transports.gouv.qc.ca/per/0937584/01_2005.pdf, 2005.

[40] Packer3d. Quebec vehicle load standards. http://www.packer3d.com/node/583. Accessed: 2019-07-10.

[41] K Imakura, K Yoshida, K Fukuda, Tetsuya Kinugasa, and Ryota Hayashi. Accuracy examination of an estimation method of axle weights for in-motion vehicles by using miniature experimental models. *Journal of Physics: Conference Series*, 1065:042022, 2018.

[42] K Fukuda, K Yoshida, Takayuki Ono, K Kameoka, and T Hirata. An advanced algorithm for estimating axle weights of in-motion vehicles. In *Proceedings of 19th International Conference on Force, Mass & Torque, IMEKO TC3, Cairo, Egypt*, 2005.

[43] Reynolds, W. R. and Hertel J. E. and Rutkowski. K. R. . Weigh-in-motion scale. US Patent 8736458 B2, 2011.

[44] Liu C. R., Guo L., Li J., and Chen X. Weigh-in-motion (WIM) sensor based on em resonant measurements, 2007.

[45] Bowie J. M. *Development of a Weigh-In-Motion system using acoustic emission sensors*. PhD thesis, University of Central Florida, 2011.

[46] Bajwa R. *Wireless Weigh-In-Motion: using road vibrations to estimate truck weights*. PhD thesis, University of California, Berkeley, 2013.

[47] Chongfeng Wei and Hamid Taghavifar. A novel approach to energy harvesting from vehicle suspension system: Half-vehicle model. *Energy*, 134:279 – 288, 2017.

[48] Vittore Cossalter. *Motorcycle dynamics*. LULU, ISBN: 9781447532767, 2006.

[49] Subaru Truck. Specification of Sambar truck. https://www.subaru.jp/sambar/truck/spec/spec.html. Accessed: 2019-07-10.

[50] Karl Hoffmann. Applying the Wheatstone bridge circuit. *HBM, Darmstadt*, 2001.

Appendix A

Experimental site

(a) The experimental location

(b) Actual experimental site

Fig. A.1 The experimental site

Appendix B

List of publication

Journal paper

1. Pham X.T, Okuma M., Bur M., and Abidin Z., An estimation method for pavement weigh-in-motion system with preliminary experiment, JSME Mechanical Engineering Journal, Vol.7, No.6, 2020, doi: 10.1299/mej.20-00405

2. Pham X.T, Okuma M., Bur M., and Abidin Z., Basic study on weigh-in-motion of vehicles in acceleration and deceleration, JSME-2021, JSME Mechanical Engineering Journal, in press.

International conference

1. Pham X.T, Okuma M., Bur M., and Abidin Z., A basic study toward the establishment of Weigh in Motion, Oral presentation, 4th International Conference on Vibro-Impact System (ICOVIS), Kassel, Germany, 2018.